Systematics of carbon- and oxygen-induced fusion on nuclei with $12 \leq A \leq 19$

D. G. Kovar, D. F. Geesaman, T. H. Braid, Y. Eisen,* W. Henning, T. R. Ophel,† M. Paul, K. E. Rehm,‡ S. J. Sanders, P. Sperr,§ J. P. Schiffer, S. L. Tabor,‖ S. Vigdor,¶ and B. Zeidman
Argonne National Laboratory, Argonne, Illinois 60439

F. W. Prosser, Jr.
Argonne National Laboratory, Argonne, Illinois 60439
and University of Kansas, Lawrence, Kansas 66045

(Received 11 June 1979)

Measurements of the total fusion cross sections for $^{12}C + ^{12}C$, ^{13}C, ^{14}N, ^{15}N, ^{16}O, ^{18}O, and ^{19}F and $^{16}O + ^{16}O$ have been performed over the energy range from 1.5 to 3 times the Coulomb barrier energy. Fusion barrier parameters were extracted for each system. Three systems, $^{12}C + ^{12}C$, $^{12}C + ^{16}O$, and $^{16}O + ^{16}O$, show rather pronounced oscillatory structure in the energy dependence of the fusion cross sections. The maximum fusion cross sections for the systems studied vary by as much as 10–20%, depending on the particular entrance channel. The specific structure of the interacting nuclei clearly does have an effect; the fusion process is not entirely dominated by the macroscopic features of the ion-ion interaction.

[NUCLEAR REACTIONS, fusion, measured $\sigma_{\text{fusion}}(E)$; $^{12}C+^{12}C$, $7.4 \leq E_{c.m.} \leq 31.2$ MeV; $^{12}C+^{13}C$, $7.6 \leq E_{c.m.} \leq 24.9$ MeV; $^{12}C+^{14}N$, $15.1 \leq E_{c.m.} \leq 24.0$ MeV; $^{12}C+^{15}N$, $8.9 \leq E_{c.m.} \leq 26.7$ MeV; $^{12}C+^{16}O$, $12.9 \leq E_{c.m.} \leq 27.0$ MeV; $^{12}C+^{18}O$, $11.9 \leq E_{c.m.} \leq 28.0$ MeV; $^{12}C+^{19}F$, $11.6 \leq E_{c.m.} \leq 27.1$ MeV; $^{16}O+^{16}O$, $14.9 \leq E_{c.m.} \leq 36.0$ MeV; deduced fusion barrier parameters.]

I. INTRODUCTION

A great deal of interest has recently focused on the fusion cross sections in heavy-ion reactions for target-projectile systems involving $1p$-shell and $2s$-$1d$-shell nuclei. This interest was motivated to a large extent by the observation of two unexpected features in the fusion cross section excitation function, $\sigma_{\text{fus}}(E)$. The first was the observation[1,2] of oscillatory structures in $\sigma_{\text{fus}}(E)$ for some systems (e.g., $^{12}C+^{12}C$ and $^{16}O+^{12}C$) but not for others. Second was the observation[2-4] of significantly different maximum fusion cross sections, $\sigma_{\text{fus}}^{\max}$, for systems differing by only a nucleon. These features suggest that the detailed structure of the nuclei plays an important role in fusion; one had expected fusion to depend on the macroscopic properties of the nuclei involved. To investigate these features in more detail, fusion cross sections have been measured for a number of systems with $12 \leq A_{\text{proj,targ}} \leq 19$. In Sec. II, the experimental method will be discussed and the data will be presented in Sec. III. In Sec. IV, the present results will be discussed in the context of the systematics established by these and other measurements, and in the framework of the macroscopic models that have been proposed. The emphasis of the discussion will be on establishing the evidence for microscopic effects (i.e., structure effects) in the behavior of the fusion cross section. Section V will summarize the conclusions reached in this study.

II. EXPERIMENTAL TECHNIQUE AND DETAILS

The beams used in this study were obtained from the Argonne National Laboratory (ANL) FN tandem accelerator. The measurements were performed in the ANL-70-inch scattering chamber where the beams were tightly constrained by collimators. The systems studied and the energy ranges over which measurements were made are shown in Table I. In all the reactions involving ^{12}C, the targets were self-supporting carbon foils of ≈ 20–40 $\mu g/cm^2$ thickness. In the study of the $^{16}O+^{16}O$ reaction, the target consisted of Al_2O_3 foils of thickness ≈ 50 $\mu g/cm^2$.

The fusion cross sections were measured by detecting the heavy fragments (e.g., the evaporation residues) resulting from compound nucleus formation and subsequent particle evaporation. The nuclear charge Z of the individual reaction products was identified by means of the measurement of the differential energy loss ΔE. A conventional silicon surface-barrier ΔE-E telescope (employing either a 2.3 μm or a 3.6 μm ΔE detector) or a gas-ionization chamber-silicon detector telescope[5] was used as indicated in Table I. Electropolished tantalum slits (of thickness ≈ 0.005 inch) were used to define the solid angle. The solid angle varied over the range 2–13×10^{-6} sr corresponding to target-detector distances between 50 and 20 cm.

The fusion telescope allowed for simultaneous detection of elastic scattering events and the

TABLE I. List of the systems for which fusion cross sections were measured in the present study and the energy range over which measurements were performed, either with (1) a silicon surface barrier $\Delta E - E$ telescope or (2) a gas ionization chamber-silicon detector telescope.

System	Energy range	Detector system
$^{12}C+^{12}C$	$7.4 \leq E_{c.m.} \leq 31.2$ MeV	1
$^{12}C+^{13}C$	$7.6 \leq E_{c.m.} \leq 24.9$ MeV	2
$^{12}C+^{14}N$	$15.1 \leq E_{c.m.} \leq 24.0$ MeV	2
$^{12}C+^{15}N$	$8.9 \leq E_{c.m.} \leq 26.7$ MeV	2
$^{12}C+^{16}O$	$12.9 \leq E_{c.m.} \leq 27.0$ MeV	1
$^{12}C+^{18}O$	$11.9 \leq E_{c.m.} \leq 28.0$ MeV	1
$^{12}C+^{19}F$	$11.6 \leq E_{c.m.} \leq 27.1$ MeV	1
$^{16}O+^{16}O$	$14.9 \leq E_{c.m.} \leq 36.0$ MeV	2

evaporation residues. Data were stored in a two-dimensional E vs ΔE matrix; representative spectra obtained in the two $\Delta E - E$ telescope systems are shown in Figs. 1 and 2. In several measurements, the ΔE resolution was sufficient to identify groups of different Z. The spectra contain all events for which a ΔE signal above some lower threshold was obtained, including all events for which there were no E signals (i.e., evaporation residues which were stopped or which were multiple scattered in the ΔE detector and did not reach the E detector; such events were found to be a negligibly small fraction of the fusion strength except at the lowest energies).

For reactions involving a ^{12}C target, all events with Z greater than that of the incident ion were included as fusion. Uncertainties arising from

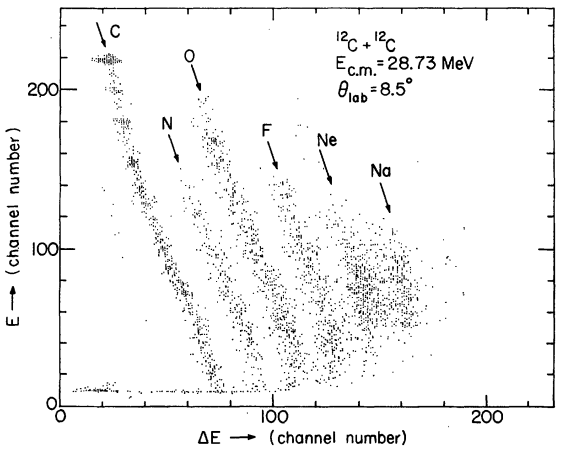

FIG. 1. Representative ΔE-E two-dimensional plot obtained for the $^{12}C+^{12}C$ system using the silicon surface barrier ΔE-E detector system (3.6 μm ΔE detector).

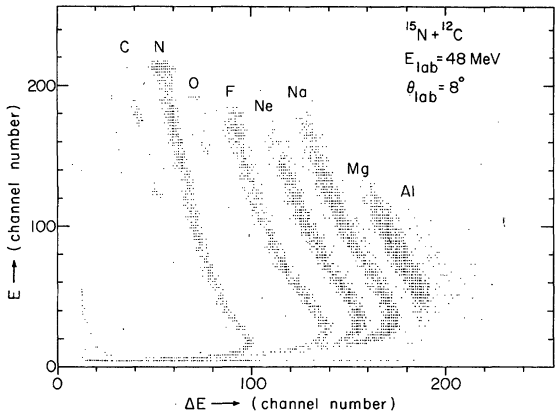

FIG. 2. Representative ΔE-E two-dimensional plot obtained for the $^{12}C+^{14}N$ system using the gas ionization detector-silicon detector telescope system.

this procedure and the method for identifying the fusion yields in the $^{16}O+^{16}O$ reaction will be discussed later. The angular distributions of the fusion products are strongly forward peaked and were in general measured over the angular range $2° \lesssim \theta_{lab} \lesssim 30°$ which corresponds roughly to 2–3 orders of magnitude in cross section. Of primary importance in establishing the total cross section were the yields in the angular region $\approx 4°$–$8°$ which corresponds to the maximum in $(d\sigma/d\Omega)\sin\theta$.

Relative normalizations of the elastic and fusion angular distributions were obtained using the beam current integrator as well as the monitors placed symmetrically left and right ($\pm 10°$) of the beam. These monitors were also used to monitor the beam direction. The beam direction and hence the ΔE–E telescope angle were established to $\lesssim 0.02°$ from measurements on opposite sides of the beam. The absolute normalization of the fusion cross section angular distribution at each energy was determined from a comparison of the yields of the fusion (N_{fus}) and elastically scattered (N_{el}) events detected in the telescope at forward angles ($\theta_{lab} \cong 3$–$10°$),

$$\left(\frac{d\sigma_{fus}}{d\Omega}\right)_{lab} = \frac{N_{fus}}{N_{el}} \left(\frac{d\sigma_{el}}{d\Omega}\right)_{lab}. \quad (1)$$

While the elastic scattering at these forward angles is generally very nearly Rutherford scattering, optical model calculations were used to establish accurately the elastic scattering cross section. The optical model parameters[6-9] used are referenced in the tables listing the fusion cross sections. While complete angular distributions of the evaporation residues were measured at several energies, excitation functions were measured in many cases in finer steps at a fixed angle near the

maximum in $(d\sigma/d\Omega)\sin\theta$. Since the shapes of the fusion angular distributions change smoothly as a function of bombarding energy, the measured angular distributions were used to interpolate the total fusion cross sections, σ_{fus}, from the single angle yields measured at the intermediate energies. In Tables II–IX, the energies at which full angular distributions were measured are indicated.

The uncertainties in the total fusion cross sections arise from statistics, identification of fusion yields, extrapolation of the measured angular distribution into the range of 0°–2°, and the normalization procedure. In the measurements reported here, the statistical uncertainties are $\lesssim 1$–3%. The uncertainties arising from the extrapolation procedure to $\theta_{lab} = 0°$ are believed to be $\lesssim 1\%$ in the great majority of the cases. The identification procedure can potentially be a larger source of error at the lowest and highest incident energies. At the lowest energies, the evaporation residues for some of the systems fall into the region of the elastic tail. An extrapolation procedure was employed to extract these yields and the resulting uncertainties were estimated to be $\lesssim 3\%$. At the highest incident energies, the evaporation residues may appear with a Z less than or equal to that of the projectile[10] and hence were not included in our operational definition of fusion yields. However, unless specifically discussed, there was no evidence of significant strength in the $Z \lesssim Z_{projectile}$ groups even at the highest energies. Finally, there is some reaction strength in the region of $Z > Z_{projectile}$ which arises from quasi-elastic direct reactions. In cases where such direct strength was obvious in the data, it was excluded. In other cases, estimates of the direct contributions were obtained using DWBA calculations and the shapes of the observed energy spectra. Unless specifically discussed in the following sections, the uncertainties in the identification procedure were estimated to be of the order of ~1–3%. The uncertainties in the normalization procedure used in establishing the relative fusion cross sections from single angle measurements were estimated to be $\lesssim 3\%$ unless otherwise noted. As discussed above, we have operationally defined the fusion cross section to be the sum of the cross sections for all elements with $Z > Z_{projectile}$ except for certain discrete contributions which result from direct transfer reactions. The dominant uncertainty in *these* fusion cross sections arises from the uncertainties in unambiguously establishing the absolute cross section for the elastic scattering; the most severe problems come at highest energies where even at forward angles, there begins to be a sensitivity to the choice of optical model parameters. In general, with our definition of the fusion cross section, the relative errors are believed to be $\lesssim 3\%$ and the absolute uncertainties of the order of $\lesssim 5\%$ for most systems.

TABLE II. Total and elemental fusion cross sections obtained for the $^{12}C + ^{12}C$ system. The underlined energies indicate the energies at which the fusion cross section was established from full angular distributions; at other energies, single-angle ($\theta_{lab} = 6°$) data were used. Optical model parameters of Ref. 6 were used in normalizing the fusion data to elastic scattering.

$E_{c.m.}$ (MeV)	σ^Z_{fus} (mb) [a] N	O [c]	F	Ne	Na	σ^{tot}_{fus} (mb)	$\Delta\sigma_{fus}$ [b] (mb)
7.44		118				286	±20 [d]
8.70						392	20 [d]
9.32						551	20
9.95		260				577	17
10.58						587	25
11.20		288				594	18
11.83						670	25
12.46		370				701	22
13.08						740	25
13.71	<5	430	28	148	140	747	24
14.33						859	30
14.96	≤5	500	44	156	151	856	21
15.00						838	25
15.59						875	30
16.21	5	495	52	124	167	843	22
16.84						861	28
17.46	~8	513	71	104	159	855	25
18.09						844	26
18.72	~10	521	93	84	160	867	22
19.34						907	26
19.97	~15	544	103	89	155	906	22
20.59						956	29
21.22	23	558	107	98	149	935	21
21.84						917	28
22.47	36	490	117	87	144	874	23
23.09						843	25
23.72	49	456	125	100	132	862	21
24.35						832	25
24.97	65	454	132	113	114	878	24
25.60						879	25
26.22	70	452	133	118	95	868	23
26.85						835	30
27.47	86	404	141	116	87	834	22
28.72	106	341	135	112	72	766	20
29.98	130	290	129	118	59	726	21
31.23						716	26

[a] Uncertainties of the elemental cross sections are ~5% for the strong groups and can be as large as 50% for the weaker groups due to systematic uncertainties in resolving the Z groups.

[b] Relative errors are listed; absolute errors are ~5% unless otherwise indicated.

[c] For $E_{c.m.} < 13$ MeV, only the oxygen elemental yields could be unambiguously identified.

[d] Absolute errors 10%.

III. EXPERIMENTAL RESULTS

A. $^{12}C + ^{12}C$ system

The fusion cross sections for the $^{12}C + ^{12}C$ system were measured over the energy range $7.4 \lesssim E_{c.m.} \lesssim 31.2$ MeV.[2] A representative $\Delta E - E$ spectrum is shown in Fig. 1 and examples of the angular distributions for the evaporation residues are shown in Fig. 3. The total fusion cross sections, based on the full angular distributions and on the single angle ($\theta_{lab} = 6°$) measurements, are listed in Table II. The errors associated with the fusion cross sections in Table II arise primarily from uncertainties in accurately normalizing the elastic scattering at forward angles. Not included in the errors are possible systematic errors arising from the identification of the evaporation residues. An estimate of the direct strength contributing to the observed yield with $Z > 6$ gives $\lesssim 10$ mb, although the possibility of somewhat larger strength cannot be excluded at the higher bombarding energies. Also, at the higher bombarding energies (i.e., $E_{c.m.} \gtrsim 20$ MeV) evaporation leading to residues with $Z \leq 6$ may be possible, although the energy spectra for $Z \leq 6$ groups show no indication of such events.

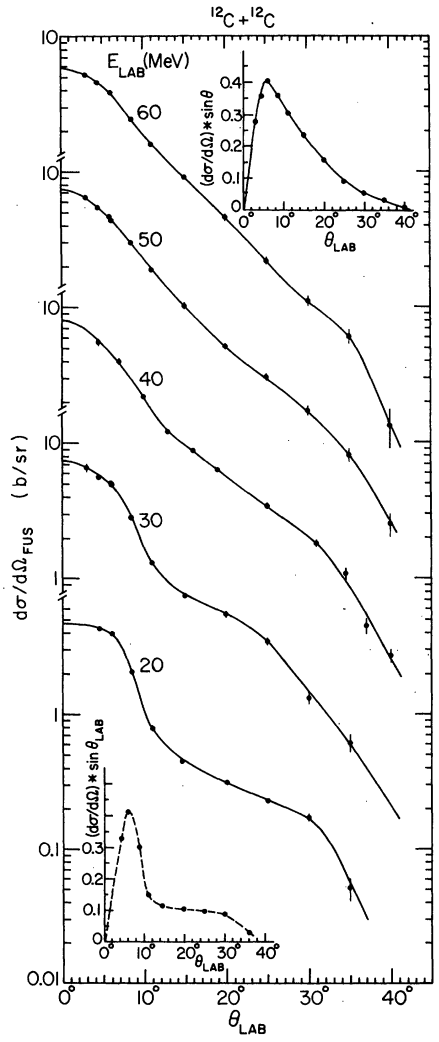

FIG. 3. Angular distributions of the evaporation residues observed at bombarding energies $E_{lab} = 20$, 30, 40, 50, and 60 MeV for the $^{12}C + ^{12}C$ system. The inserts are plots of $(d\sigma/d\Omega)*\sin\theta$ at $E_{lab} = 20$ and 60 MeV.

The partial and total fusion cross section excitation functions measured for the $^{12}C + ^{12}C$ reaction are shown in Fig. 4; for energies $E_{c.m.} \lesssim 13$ MeV the ΔE resolution was not sufficient to resolve the individual Z groups. Clear oscillatory structures in the total fusion cross sections are observed as function of bombarding energy. The maxima appear at about 5.5 MeV intervals at $E_{c.m.} \approx 10.0$, 15.5, 21.0, and 26 MeV. The measured partial fusion cross sections show that these structures are due primarily to the oxygen and neon evaporation residues. Based on measurements for other systems,[11] where it has been established that the structures are present in the α-removal channels, it is suggested that the channels showing the oscillatory behavior in the $^{12}C + ^{12}C$ reaction are the ^{20}Ne and ^{16}O channels. In Fig. 5, the total fusion cross sections are plotted for comparison with the other systems measured in this study.

The total fusion cross sections established in the present measurements are plotted in Fig. 6 as a function of $1/E_{c.m.}$. Also shown are the cross sections established by Namboodiri, Chulick, and Natowitz[12] in charged-particle measurements at high energies. Measurements at lower bombarding energies were performed by Spinka and Winkler[13] and Erb, Betts, and Bromley[14]. These latter cross sections were obtained in γ-ray measurements and, while the relative errors are small and the fine structure present in the excitation function is clearly defined, the uncertainties in the absolute cross sections are $\approx 50\%$ and these data are not shown in Fig. 6. Also, Conjeaud *et al.*[15] have recently reported results of measurements over the energy range $14 \lesssim E_{c.m.} \lesssim 27$ MeV. As discussed in their paper, there is good agreement with our results except at the higher energies where their absolute cross sections are ~50–100 mb smaller. (At lower energies, the question of what constitutes fusion products was addressed by Conjeaud *et al.*[15] with specific reference to the $^{12}C + ^{12}C \rightarrow \alpha + ^{20}Ne$ reactions. Whether this channel is to be regarded as a direct channel or as pre-equilibrium fusion, for example, is not clear at this time. In the present study, it is included in

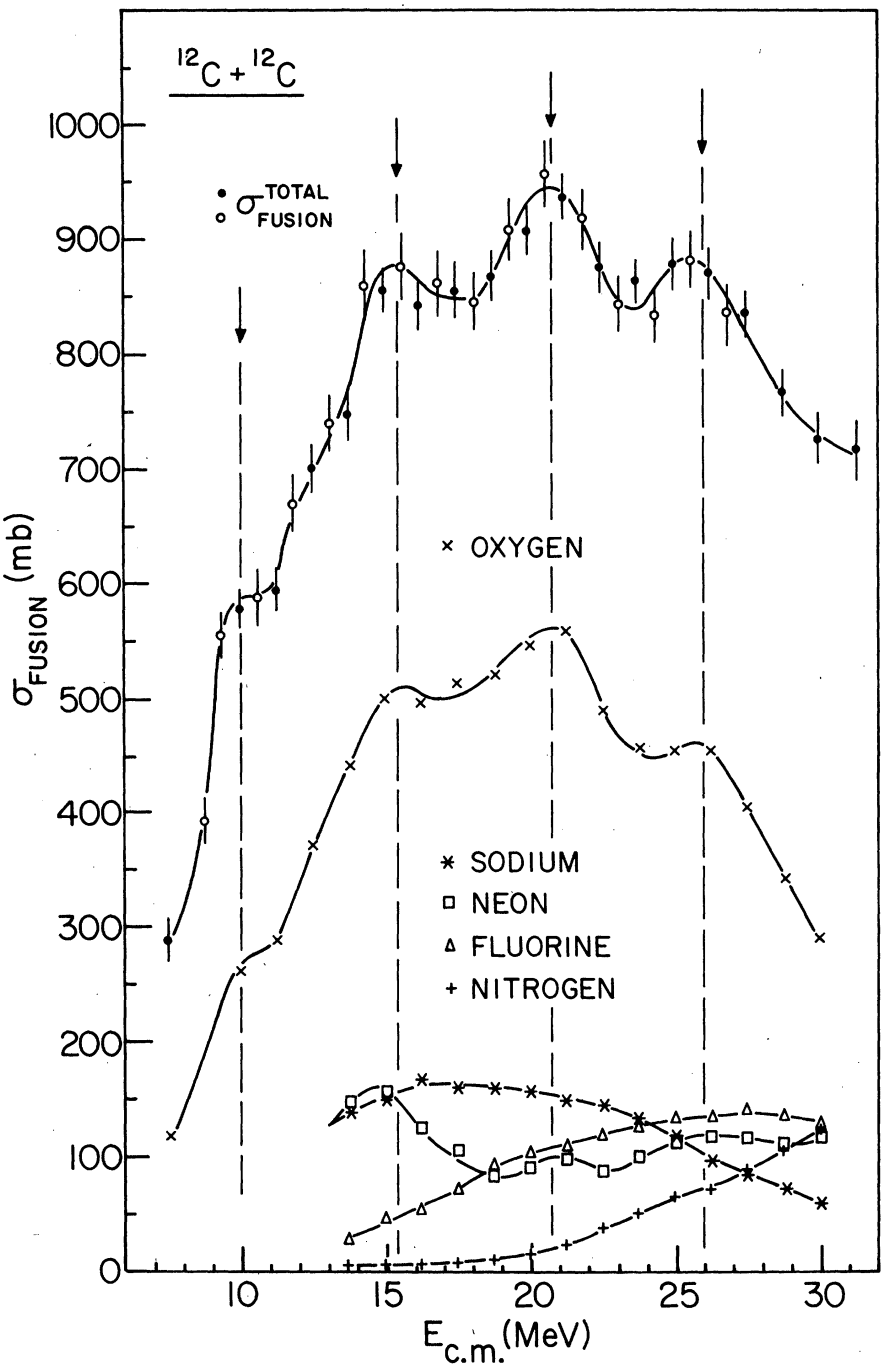

FIG. 4. Partial and total fusion cross section excitation functions measured for the $^{12}C + ^{12}C$ system. The solid and open circles represent cross sections established from full angular distribution and single-angle measurements, respectively.

the fusion cross sections.) It should also be noted that in the energy range $E_{c.m.} = 14-16$ MeV, Conjeaud *et al.*[15] performed measurements in small energy steps and found more detailed structure than indicated by the present data. These recent results of Conjeaud are not shown in Fig. 6.

While the measurements of Namboodiri, Chulick, and Natowitz[12] at the highest energies are consistent with the trend indicated by the present measurements, their cross sections at $E_{c.m.} = 22.5$ MeV and 37.5 MeV are $\simeq 100-300$ mb larger than those observed in the present study and also

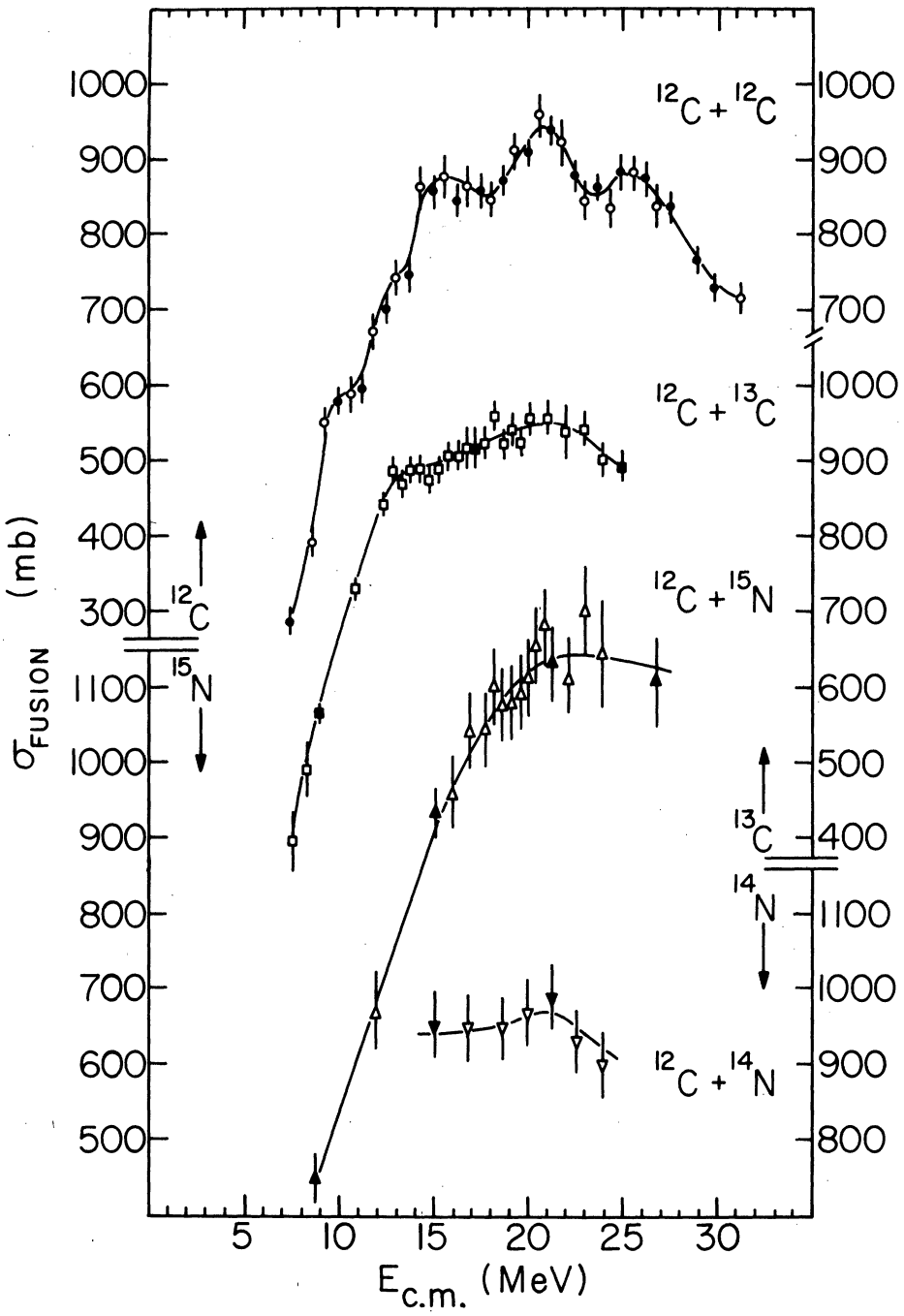

FIG. 5. Total fusion cross section excitation functions for the $^{12}C+^{12}C$, $^{13}C+^{12}C$, $^{14}N+^{12}C$, and $^{15}N+^{12}C$ systems. The solid and open symbols represent cross sections established from full angular distribution and single-angle measurements, respectively.

those of Ref. 15. Since carbon production from the decay of the compound system is expected to become important at energies above $E_{c.m.} \approx 20$ MeV, this disagreement is partly a result of inclusion of only the yields for $Z>6$ in our cross section. This, however, is not the complete explanation. At $E_{c.m.} = 22.5$ MeV, for example, Namboodiri, Chulick, and Natowitz[12] quote $\sigma_{fus} = 1020 \pm 100$ mb for $Z>6$ compared to $\sigma_{fus} = 874 \pm 44$ mb in the present study. (Their estimate of strength for $Z \leq 6$ was $\lesssim 30$ mb.) Similarly at $E_{c.m.} = 37.5$ MeV, their σ_{fus} for $Z>6$ is larger than that

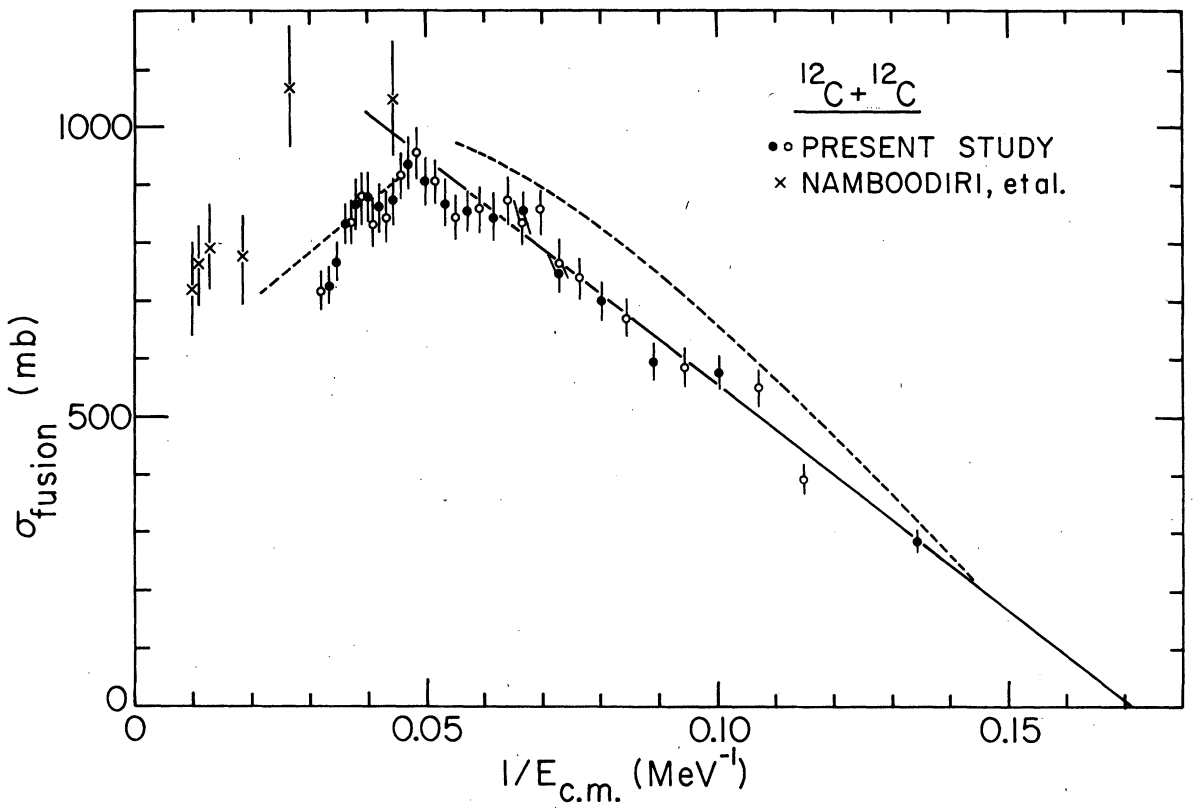

FIG. 6. Total fusion cross sections established in this study for the $^{12}C+^{12}C$ system plotted versus $1/E_{c.m.}$. The solid and open circles represent cross sections established from full angular distribution and single-angle measurements, respectively. Also shown are the results of Namboodiri, Chulick, and Natowitz (Ref. 12). The solid line represents a least-squares fit of the expression $\sigma_{fus}=\pi R_B^2(1-V_B/E)$ to the data. The dashed curve represents Bass model predictions (see text).

implied by the trend of our results. Further measurements are necessary to resolve these discrepancies.

B. $^{12}C+^{13}C$ system

The fusion yields in the $^{12}C+^{13}C$ reaction were measured over the energy range $7.6 \leq E_{c.m.} \leq 24.4$ MeV. The total fusion cross sections based on the full angular distribution measurements and the single angle ($\theta_{lab}=5°$) measurements are listed in Table III. For $E_{c.m.}>17$ MeV, the yield for each element was clearly separated; at lower energies it was not possible to completely separate the Mg and Na yields. The elemental distributions for $Z>6$ are listed in Table III. As can be seen in Fig. 5, no pronounced oscillatory structures are observed in the excitation function for the total fusion cross section. In Fig. 7, the total fusion cross sections are plotted versus $1/E_{c.m.}$. Measurements of Dayras *et al.*[16] performed at lower bombarding energies are in excellent agreement with the present work in the region of overlap; this is probably somewhat fortuitous, however, since the absolute errors of the cross sections are quoted by Dayras *et al.* to be ±30%. They also see some evidence of structure in an energy range not studied in detail here.

C. $^{12}C+^{14}N$ system

Fusion cross sections for the $^{12}C+^{14}N$ system were measured over the energy range 15.1 MeV $\leq E_{c.m.} \leq 24.0$ MeV. Of primary interest was to establish the maximum fusion cross section, σ_{fus}^{max}, for comparison with that observed for the $^{12}C+^{15}N$ system. The total fusion cross sections from the full angular distribution measurements and the single angle measurements ($\theta_{lab}=6°$) are listed in Table IV. The ΔE resolution permitted identification of the elemental yields, and the cross sections for $Z>7$ are also listed in Table IV. The total fusion cross sections are plotted versus $E_{c.m.}$ in Fig. 5, where it can be seen that the behavior is consistent with a smooth energy dependence. In Fig. 8, the cross sections are

TABLE III. Total and elemental fusion cross sections obtained for the $^{12}C+^{13}C$ system. The underlined energies indicate the energies at which the fusion cross sections were established from full angular distributions; at other energies, single-angle ($\theta_{lab}=5°$) data were used. The optical model parameters used to normalize the fusion data to elastic scattering were $V=12.2$ MeV, $V_I=4.1$ MeV, $r_0=1.34$ fm, $r_{I0}=1.47$ fm, $a=0.59$ fm, and $a_I=0.58$ fm.

$E_{c.m.}$ (MeV)	σ^Z_{fus} (mb) [a] N	O	F	Ne	Na	Mg	σ^{tot}_{fus} (mb)	$\Delta\sigma_{fus}$ [b] (mb)
7.62		42		141	211 [c]		394	±40 [d]
8.35		15		215	260		490	35 [d]
9.02		37		267	258		564	13
10.95		106		324	304		734	12
12.40		189	2	360	292		843	18
12.88		204	1	398	282		885	21
13.36		204	2	366	296		868	19
13.84		242	6	342	296		886	19
14.32		274	6	331	276		887	16
14.80		281	12	323	260		876	17
15.28		278	15	329	264		886	18
15.77		332	17	311	247		907	19
16.25		336	18	311	247		912	20
16.73		348	29	301	238		916	30
17.21		366	32	278	213	27	916	30
17.70		375	41	280	203	24	923	19
18.18		422	38	278	203	18	959	19
18.66		395	48	267	193	20	923	20
19.14		401	62	258	196	27	944	22
19.62		419	61	247	177	21	925	20
20.10		445	55	251	184	21	956	23
21.06		481	73	212	177	16	959	23
22.62		475	83	217	147	16	938	±40
22.98		499	102	181	148	13	943	21
23.94	10	468	97	173	140	13	900	21
24.91	19	458	116	154	134	12	893	19

[a] Uncertainties of the elemental cross sections are discussed in Table II.

[b] Relative errors are listed; absolute errors are 5% unless otherwise indicated.

[c] For $E_{c.m.}<17$ MeV, the summed Na + Mg cross sections are given.

[d] Absolute errors are ~10%.

plotted versus $1/E_{c.m.}$, together with results previously reported in the literature.[10,15,17-19] The values reported here are in good agreement with the charged particle measurements of Stokstad *et al.*[10] and Harar *et al.*[15] which overlap in energy. The results of Switkowski, Stokstad, and Wieland[17] and Almqvist, Bromley, and Kuehner[18,19] at lower energies are also shown in Fig. 8. These γ-ray measurements quote absolute cross section uncertainties of 25–50% and only a few representative errors are indicated in the figure.

D. $^{12}C + ^{15}N$ system

The fusion cross sections for the $^{12}C+^{15}N$ system were measured over the energy range $8.9 \leq E_{c.m.} \leq 26.7$ MeV. The measurements focused on establishing σ^{max}_{fus} and on determining whether structure was present in the excitation function. The ΔE resolution permitted extraction of elemental yields for $Z>7$ for $E_{c.m.} \geq 15$ MeV; shown in Fig. 9 is an example of the angular distributions observed for the elemental and total fusion yields. The elemental and total fusion cross sections are listed in Table V. As can be seen in Figs. 5 and 10, the fusion cross section excitation function shows no evidence of structure and establishes a lower limit on σ^{max}_{fus}. For $^{12}C+^{14}N$ and $^{12}C+^{15}N$, the values of σ^{max}_{fus} differ by ≈ 200 mb. In Fig. 11, the elemental cross sections for the two systems are shown, and it can be seen that the two distributions of fusion strength differ significantly. Evaporation calculations have been performed for these two systems[15]; the basic trends of the distributions of residue strength are predicted, but the detailed distributions are not reproduced with disagreements of the order of 100 mb. The only other measurements reported for the $^{12}C+^{15}N$ system are those of Harar[15]; the agreement with the present data is excellent as can be seen in Fig. 10.

E. $^{12}C + ^{16}O$ system

Fusion cross sections for the $^{12}C+^{16}O$ system were measured over the energy range $12.9 \leq E_{c.m.} \leq 26.9$ MeV. Examples of the angular distributions for the fusion yields have previously been reported.[1] The total fusion cross sections are tabulated in Table VI. While the ΔE resolution in the present study (using a 3.6 μm silicon detector in the ΔE-E telescope) was sufficient to resolve the elemental yields for the lower Z values (i.e., $Z \leq 11$), it was not adequate to resolve clearly the yields of the higher Z values and hence elemental yields were not extracted. Measurements establishing the elemental distribution at $E_{c.m.}=15.0$ MeV, 21.0 MeV, and 26.6 MeV have been reported elsewhere.[20] A plot of the fusion cross sections as a function of $E_{c.m.}$ is shown in Fig. 12 where the oscillatory behavior as a function of incident energy is clearly evident. Maxima can be observed at $E_{c.m.} \cong 14$, 17, 21, and 25 MeV with peak to valley differences of $\approx 10\%$.

Several other measurements for this system have been reported[11,18-32] which include charged particle measurements[20-24] and γ-ray measurements.[11,18,25-32] As noted previously, the two types of measurements have different merits. While the charged particle measurements tend to have less serious problems in establishing absolute cross sections, the γ-ray measurements are

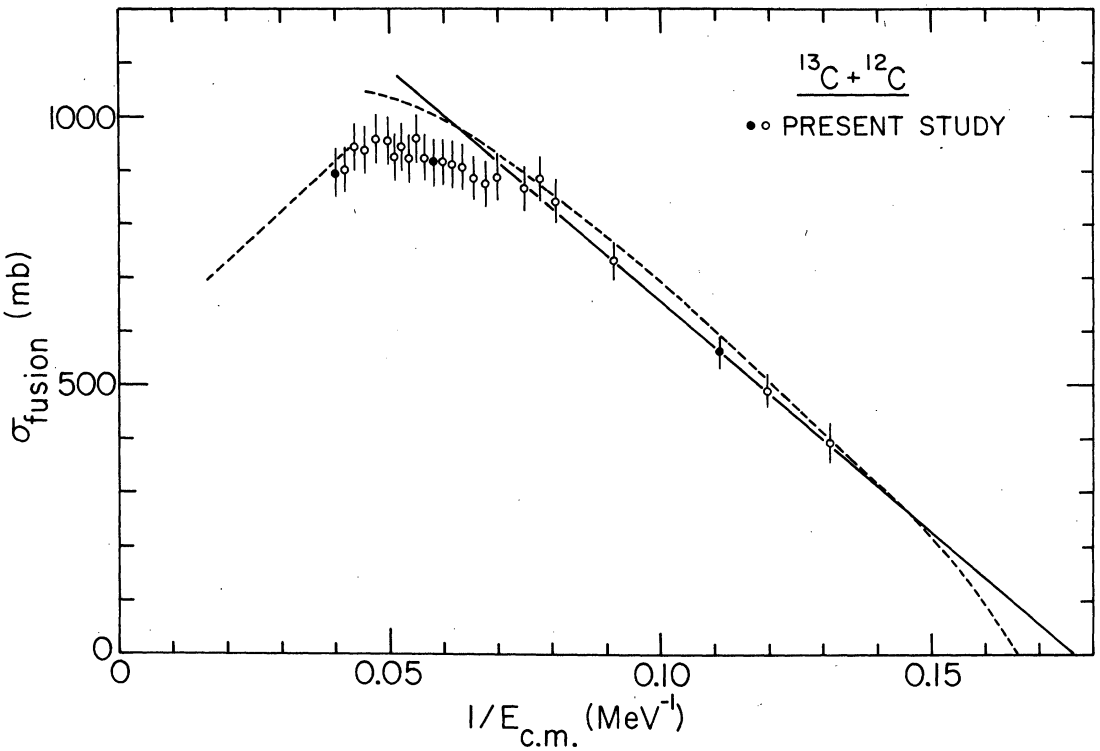

FIG. 7. Total fusion cross sections for the $^{13}C + ^{12}C$ system established in this study plotted versus $1/E_{c.m.}$. The solid and open circles represent cross sections established from full angular distribution and single-angle measurements, respectively. (For description of curves, see Fig. 6.)

more suitable for establishing fine structure in the excitation function. The structure seen in the present study is in basic agreement with that observed in the γ-ray measurements (e.g., Ref. 11).

TABLE IV. Total and elemental fusion cross sections for the $^{12}C + ^{14}N$ system. The underlined energies correspond to the energies at which full angular distributions were measured; at other energies, single-angle ($\theta_{lab} = 6°$) data were used. Optical model parameters of Ref. 7 were used to normalize the fusion data to elastic scattering.

$E_{c.m.}$ (MeV)	σ^{Z}_{fus} (mb) [a] O	F	Ne	Na	Mg	Al	σ_{fus} [b] (mb)
<u>15.11</u>	2	176	394	139	245		956
16.89	10	204	414	142	181	<1	951
18.67	30	202	432	134	148	2	948
20.00	59	214	417	147	130	2	969
<u>21.33</u>	83	226	428	136	114	3	990
22.62	116	203	384	137	91	3	934
24.00	167	182	364	109	77	2	901

[a] Uncertainties in the elemental cross sections are discussed in Table II.

[b] Relative errors are ~2.5–3.0%; absolute errors are ~5%.

In our discussion in the next section, our interest is focused on the absolute cross section values, and hence plotted in Fig. 13 are our results together with the other charged-particle measurements[22-24]; as can be seen, the agreement in the region of overlap is good. It should be noted that in recent γ-ray measurements (e.g., Ref. 11), great care has been taken to establish the absolute cross sections, and the agreement with the charged particle data is in fact rather good.

F. $^{12}C + ^{18}O$ system

The fusion cross sections for the $^{12}C + ^{18}O$ system were measured over the energy range 11.9 $\leq E_{c.m.} \leq$ 27.9 MeV. An example of an angular distribution observed for the fusion yields has been published previously.[2] The total fusion cross sections are tabulated in Table VII and plotted versus $E_{c.m.}$ in Fig. 12; no evidence of structure in the excitation function can be observed. The ΔE resolution did not permit extraction of elemental yields for higher Z values. The total fusion cross sections are plotted versus $1/E_{c.m.}$ in Fig. 14 together with the previously reported values of Eyal *et al.*[22] As can be seen, there are disagreements of the order of ~50–75 mb at the energies of overlap.

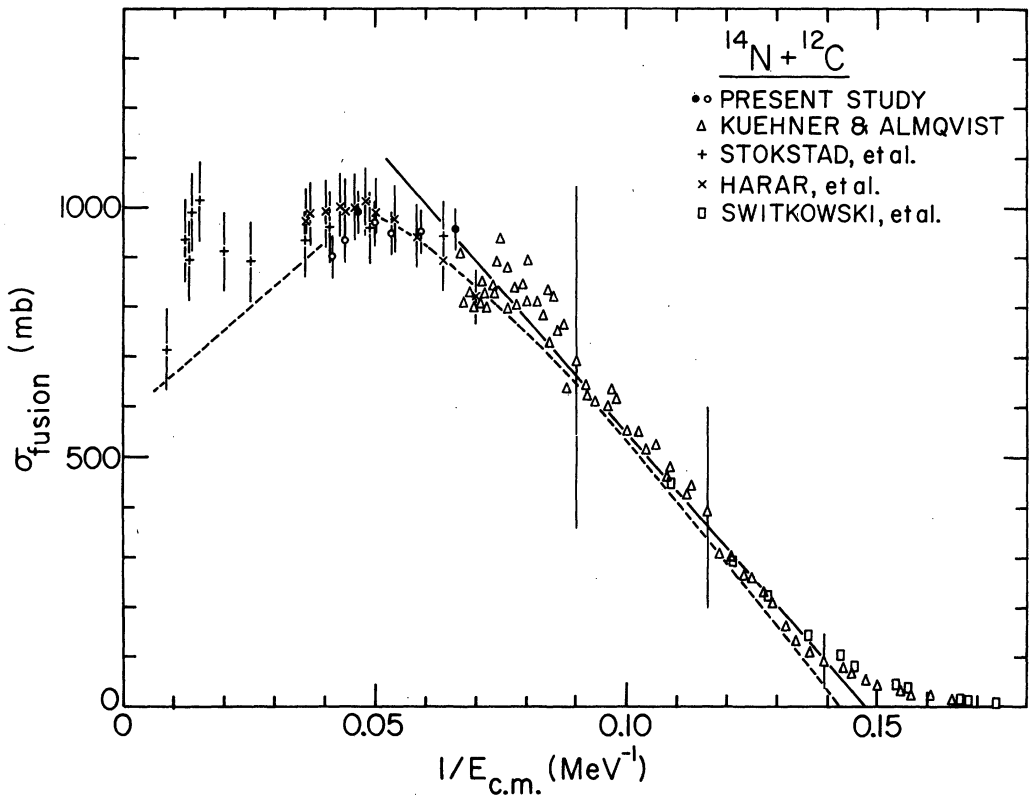

FIG. 8. Total fusion cross sections for the $^{14}N+^{12}C$ system established in this study plotted versus $1/E_{c.m.}$. The solid and open circles represent cross sections established from full angular distribution and single-angle measurements, respectively. Also shown are the results of Refs. 10, 15, 17–19. (For description of curves, see Fig. 6.)

G. $^{12}C + ^{19}F$ system

Measurements for the $^{12}C + ^{19}F$ system were performed in the energy range $11.5 \leq E_{c.m.} \leq 27.0$ MeV using the $\Delta E - E$ silicon surface barrier detector system and no elemental cross sections were extracted. An example of an angular distribution observed for the fusion yields has been published previously.[2] The fusion cross sections are listed in Table VIII and shown as function of $E_{c.m.}$ in Fig. 12. No evidence for pronounced structure in the excitation function can be seen. The total fusion cross sections are plotted versus $1/E_{c.m.}$ in Fig. 15, together with the previously reported measurement of Pühlhofer, *et al.*[33]; the agreement is good.

H. $^{16}O + ^{16}O$ system

Measurements of the fusion cross sections for the $^{16}O+^{16}O$ system were performed over the energy range 14.9 MeV $\leq E_{c.m.} \leq$ 35.9 MeV. For these studies, the problem of using an oxygen compound for the target material required a modified procedure from that described previously. At each angle, successive runs were taken with an Al_2O_3 target and an Al target. (The Al target also contained ≈ 5 $\mu g/cm^2$ oxygen, presumably due to surface oxidation.) The relative amount of oxygen and aluminum for each target was measured using the yields of resolved groups from $^{16}O+^{16}O$ and $^{16}O+^{27}Al$ elastic scattering in a monitor detector ($\theta_{lab} = 25°$). Both the elastic scattering and fusion yields for each element could be obtained by comparing the number of events in the particle telescope for each target. Since only the relative oxygen and aluminum contents of the two targets are needed for this procedure, it is not necessary to know the exact chemical composition of either target. No changes in the oxygen to aluminum ratios were observed during the course of the experiment.

A further complication for the $^{16}O+^{16}O$ measurement was the determination of the carbon content of the target, since the $^{16}O+^{12}C$ fusion reaction will populate many of the same evaporation residues as the $^{16}O+^{16}O$ reaction. To correct for this problem, the amount of carbon on the target was continuously monitored by measuring elastically

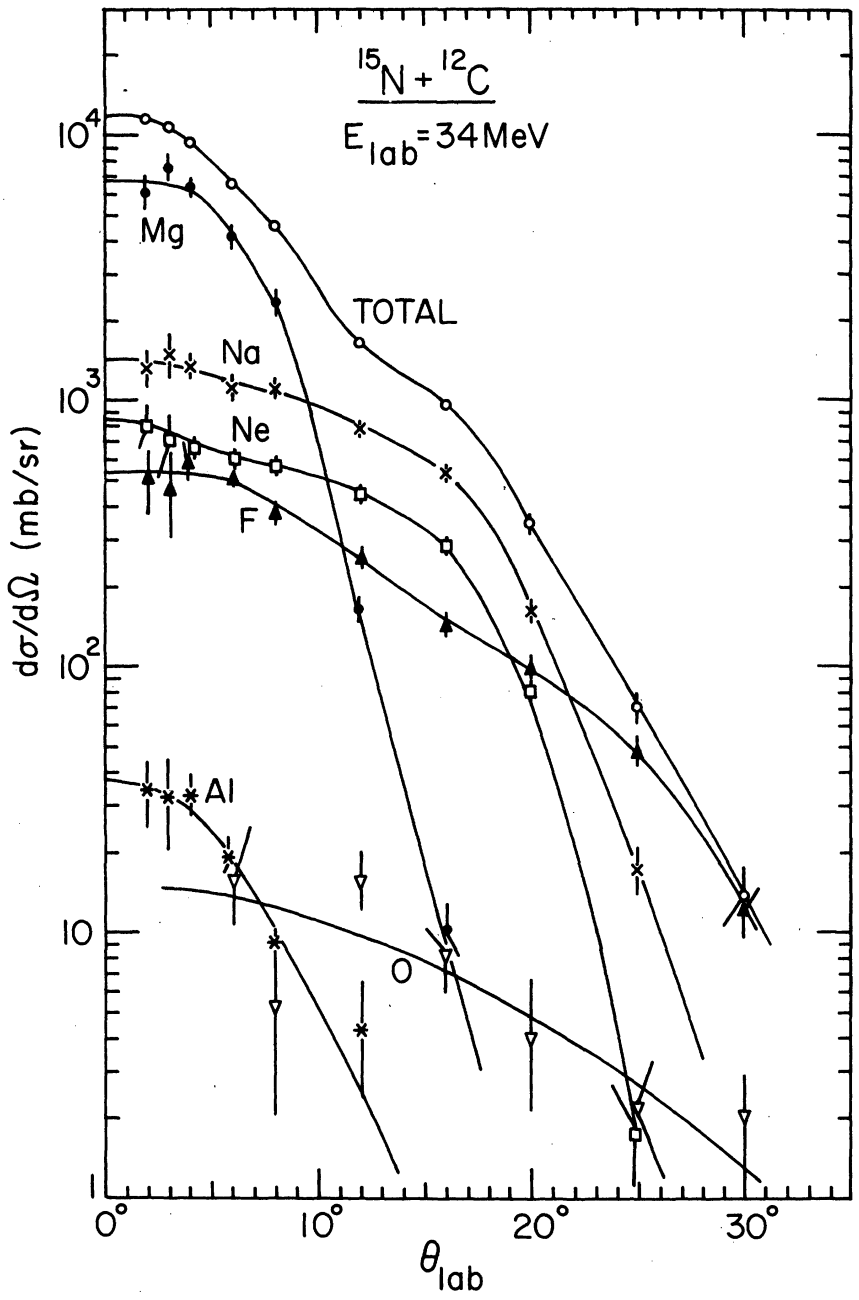

FIG. 9. Angular distributions observed for the elemental and total fusion yields for the $^{15}N+^{12}C$ system.

scattered ^{16}O and ^{12}C ions in kinematic coincidence. To minimize carbon buildup, the target was surrounded by a liquid-nitrogen-cooled copper shroud. With the shroud in place, less than 1 $\mu g/cm^2$ of carbon accumulated on the target during the course of the experiment. Even at this level, however, 2–4% corrections to the $^{16}O+^{16}O$ fusion cross sections and 1–15% corrections to the $^{16}O+^{27}Al$ fusion cross sections were required due to the carbon contamination.

The absolute normalization was established by fitting the elastic scattering from both ^{16}O and ^{27}Al with optical-model calculations using potentials taken from the literature.[8,9] A comparison of the resulting $^{16}O+^{27}Al$ fusion cross sections with previous measurements provides a good test of the subtraction procedure described above. In fact, the $^{16}O+^{27}Al$ cross sections agree well with

TABLE V. Total and elemental fusion cross sections obtained for the $^{12}C+^{15}N$ system. (See caption for Table IV.)

$E_{c.m.}$ (MeV)	σ^{Z}_{fus} (mb) [a] O	F	Ne	Na	Mg	Al	σ_{fus} [b] (mb)
8.89							453 [c]
12.00							672 [c]
15.11	4	116	146	278	371	18	933
16.00	6	140	164	273	360	19	962
16.89	9	183	173	342	318	18	1043
17.78	13	183	167	348	313	18	1042
18.22	26	200	169	371	315	20	1101
18.67	13	205	168	367	307	15	1075
19.11	23	222	174	346	299	14	1078
19.56	50	207	175	362	287	12	1093
20.00	25	221	188	384	284	13	1115
20.44	32	230	206	384	292	12	1156
20.89	30	252	198	401	287	15	1183
21.33	4	239	211	359	281	16	1127
22.22	37	229	218	339	289	7	1119 [c]
23.11	49	255	261	347	282	6	1200 [c]
23.86	48	255	249	312	274	5	1143 [c]
26.67	36	270	329	276	194	4	1109 [c]

[a] Uncertainties in the elemental cross sections are discussed in Table II.

[b] Relative errors are ~3%; absolute errors are ~5% unless otherwise indicated.

[c] Absolute errors are ~6–7%.

the published values.[34,35] The fusion cross sections established for the $^{16}O+^{16}O$ and $^{16}O+^{27}Al$ reactions are tabulated in Table IX. The errors quoted arise primarily from the uncertainties associated with the subtraction procedure and normalization. The fusion excitation function for the $^{16}O+^{16}O$ reaction is shown in Fig. 12, and there is evidence of structure similar in magnitude to that observed in the $^{16}O+^{12}C$ and $^{12}C+^{12}C$ reactions.

Five other measurements of the fusion of $^{16}O+^{16}O$ have been reported; Weidinger *et al.*,[21] Tserruya *et al.*,[36] and Fernandez *et al.*[24] performed charged particle measurements while Kolata *et al.*[37] and Cheng *et al.*[38] measured γ-ray yields. The structures observed in the present data are in basic agreement with those seen in the more sensitive γ-ray measurements. Discrepancies do exist, however, in the absolute cross sections reported in the various studies; these are shown in Fig. 16 where the excitation functions obtained in the different studies are compared. These discrepancies are much larger than those for any of the other systems studied here, and demonstrate

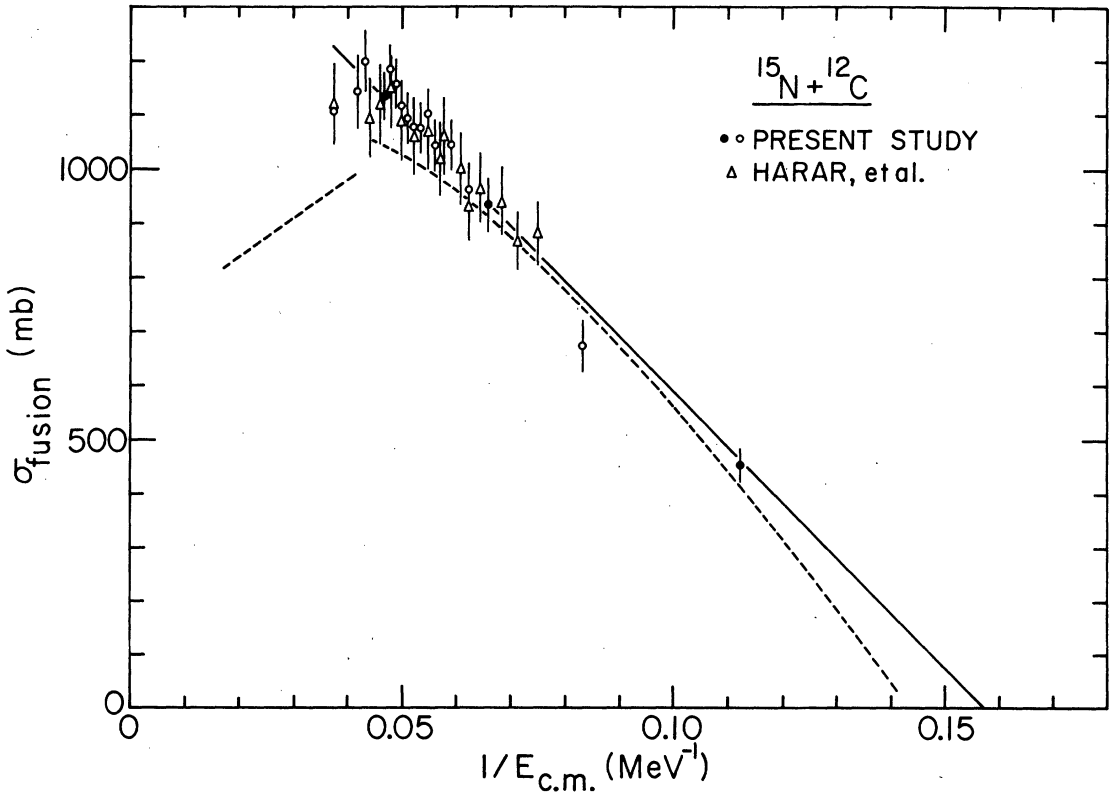

FIG. 10. Total fusion cross sections for the $^{15}N+^{12}C$ system established in this study plotted versus $1/E_{c.m.}$. The solid and open circles represent cross sections established from full angular distribution and single-angle measurements, respectively. Also plotted are the results of Ref. 15. (For description of curves, see Fig. 6.)

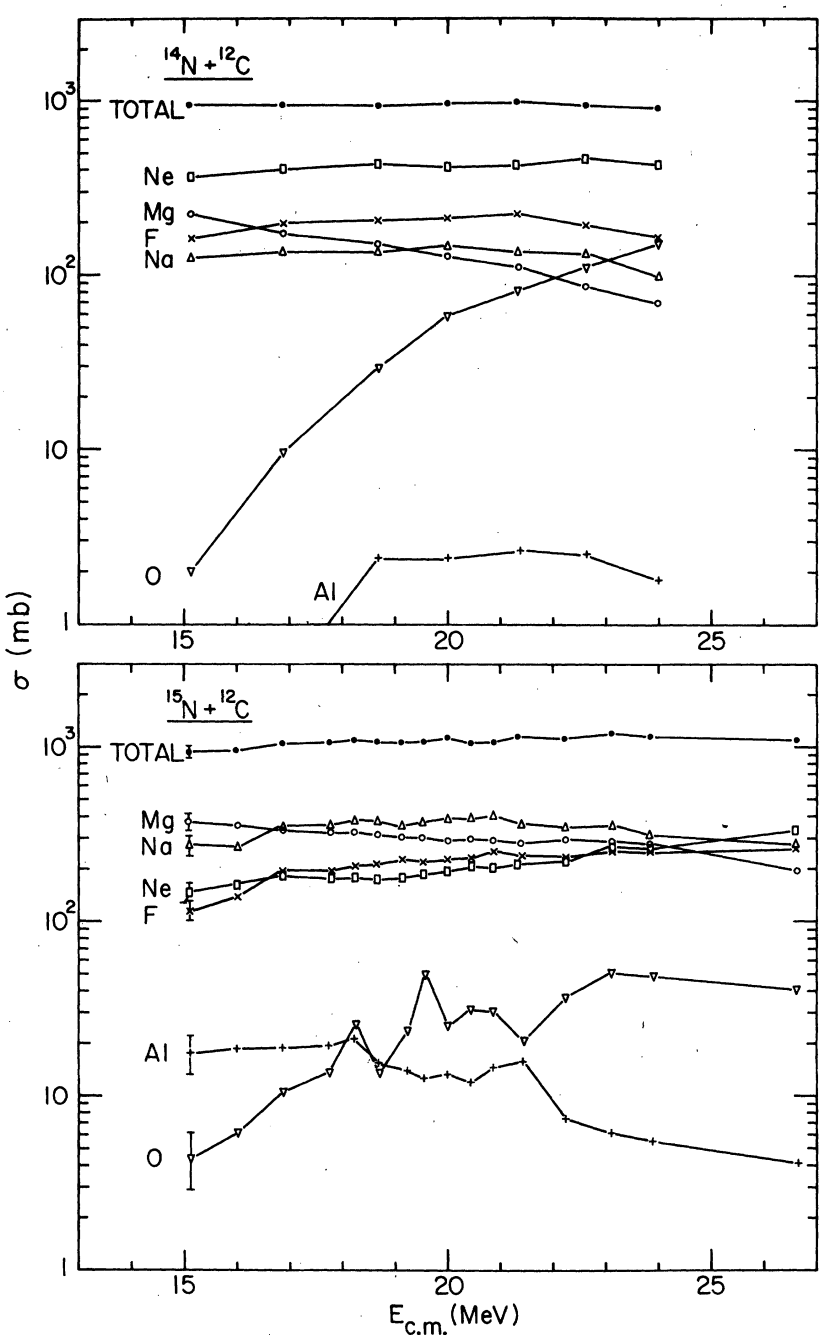

FIG. 11. Total and elemental fusion cross sections plotted versus $E_{c.m.}$ for the $^{14}N+^{12}C$ and $^{15}N+^{12}C$ systems.

the difficulty of measurements with an oxygen target. In Fig. 17, our fusion cross sections are plotted versus $1/E_{c.m.}$.

IV. DISCUSSION

A. General comments

For the energy range under consideration, the energy dependence of the fusion cross section appears to divide naturally into two regions. This division is clearly seen in plots of fusion cross sections against $1/E_{c.m.}$. There is a "low" energy region, extending from roughly 1.1 to 2.0 times the Coulomb barrier energy, where $\sigma_{fus}(E)$ is approximately linear as function of $1/E_{c.m.}$ and accounts for most of the total reaction cross section, $\sigma_{react}(E)$. In the "higher" energy region $\sigma_{fus}(E)$ often reaches a limiting or maximum value

TABLE VI. Total fusion cross sections obtained for the $^{12}C+^{16}O$ system. (See caption for Table IV.)

$E_{c.m.}$ (MeV)	σ_{fus} (mb)	$\Delta\sigma_{fus}$ [a] (mb)
12.94	729	±20
13.45	828	16
13.84	863	20
14.24	829	20
14.87	803	16
15.58	901	22
16.35	970	22
17.20	981	25
18.30	938	25
18.70	940	30
18.90	940	30
19.10	910	30
19.30	880	30
19.50	895	25
19.70	865	20
19.90	920	30
20.10	900	25
20.30	915	30
20.50	930	30
20.89	963	24
21.10	945	35
21.30	950	30
21.50	925	30
23.21	912	25
24.00	940	40
24.95	970	30
26.97	802	20

[a] Relative errors are listed; absolute errors are ~5%.

while the total reaction cross section continues to rise. The fusion cross section at "low" energies appears to be determined by the properties of the interaction barrier (i.e., by entrance channel characteristics). At "high" energies the explanation for the large difference between σ_{fus} and σ_{react} is still not fully understood. Tentative explanations fall into two basic categories: (1) The observed limitation of σ_{fus} at high energies is explained in terms of entrance channel models in which the limitation mechanism depends on Z and A of target and projectile (e.g., Refs. 39–41). (2) Alternatively, the properties of the compound nucleus formed in the reaction, and in particular the behavior of the yrast lines, are employed to impose the limitations.[15] The status of our present understanding has been the subject of several recent review articles.[42,43]

As noted in the introduction, the present study was motivated by the observation of features in $\sigma_{fus}(E)$ which suggested that the detailed structures of the interacting nuclei play an important role in the fusion process.[1-3] These were the observation of oscillatory structures in the excitation functions for some systems but not for others, and the observation of significantly different maximum fusion cross sections for systems differing by a single nucleon. The present measurements, together with similar experiments reported in the literature, form a body of data which provides an opportunity to establish the average macroscopic energy and mass dependence and to examine the extent to which individual systems show significant deviations from this average behavior. This will be done in the framework of models discussed above. The "low" energy or interaction barrier dominated region and the "higher" energy region where the limitations on σ_{fus} are observed will be discussed in Secs. IV B and IV C, respectively. The three systems showing structures in $\sigma_{fus}(E)$ will be further discussed in Sec. IV D.

B. Barrier-dominated region

It has been established that the fusion cross section behavior in the energy region between ~1 and 2 times the Coulomb barrier energy is dominated by the interaction barrier.[44] Since the fusion process is sensitive to the ion-ion potential in the region of the interaction barrier radius, it is of interest to ask whether differences in the structures of the interacting nuclei affect the potential sufficiently so as to produce observable differences in the fusion cross sections. To investigate this question we have made use of the simplest classical model which allows us to parameterize the fusion cross sections, and have looked for deviations from the average behavior established in this parametrization. In addition, the observed fusion cross sections have been compared to model predictions.

The simplest and most commonly used parametrization of fusion cross sections is the classical equation,[44]

$$\sigma_{fus}(E) = \pi R_B^2 \left(1 - \frac{V_B}{E_{c.m.}}\right). \quad (1)$$

A plot of $\sigma_{fus}(E)$ versus $1/E_{c.m.}$ allows extraction of two independent parameters, R_B (barrier radius) and V_B (barrier height). (The smooth deviation from the $1/E_{c.m.}$ behavior at lower energies results from barrier penetrability effects; Glas and Mosel,[40] using a parabolic barrier at a fixed R_B, have introduced a parametrization which incorporates, in a single functional form, the behavior of the fusion cross section from below the Coulomb barrier up to the "higher" energy region.)

In the discussion of the barrier parameters R_B and V_B which are extracted from the data using Eq. (1), it should be remembered that R_B has

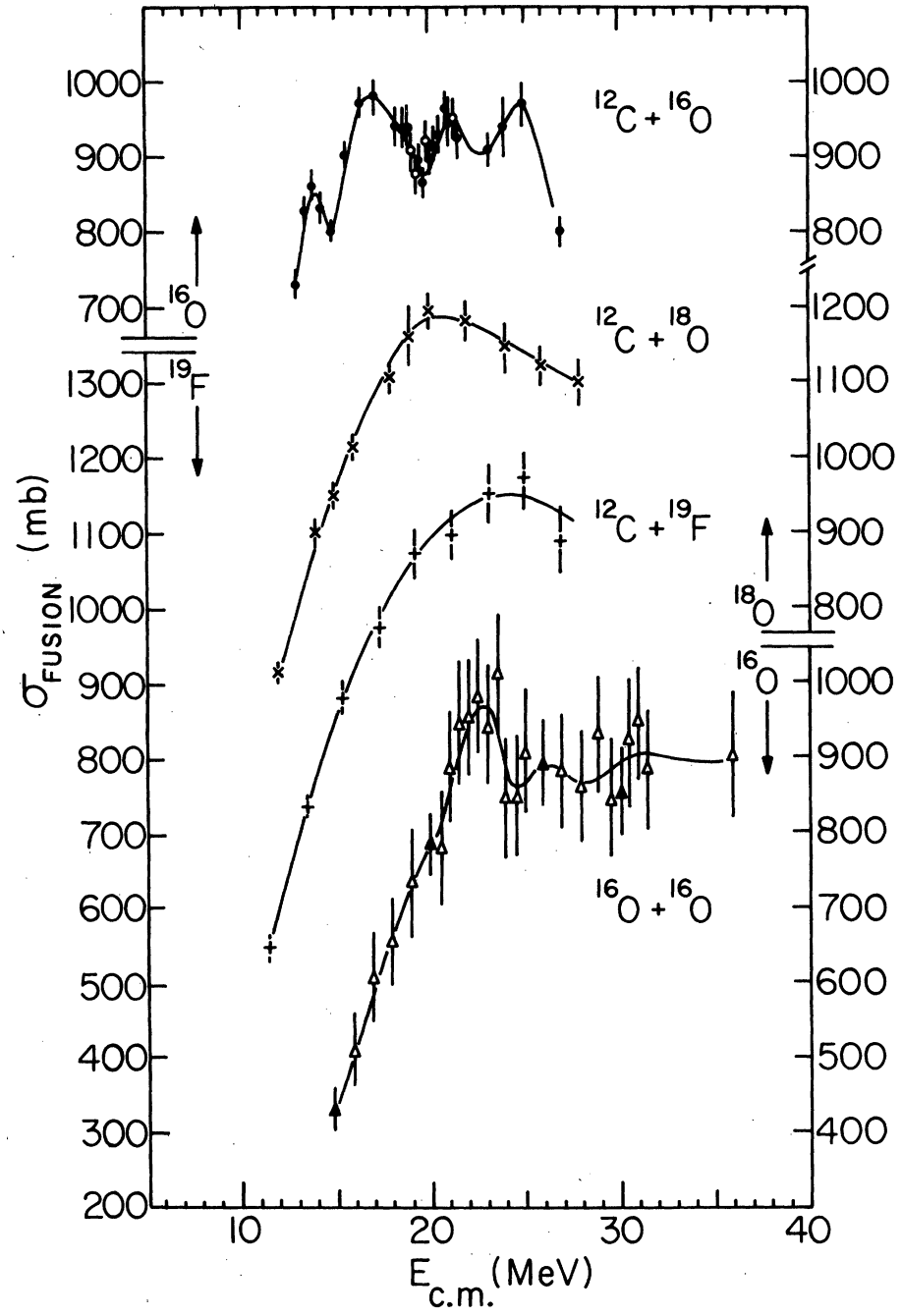

FIG. 12. Total fusion cross section excitation functions for the $^{12}C+^{16}O$, $^{12}C+^{18}O$, $^{12}C+^{19}F$, and $^{16}O+^{16}O$ systems. The solid and open symbols represent cross sections established from full angular distribution and single-angle measurements, respectively.

been assumed[40,44] to be a constant, and hence the V_B extracted should *not* be identified with the barrier potential $V_B(R)$ at R_B. If the barrier potential is assumed to be a Woods-Saxon potential with usual diffuseness, for example, the variation of R_B (and V_B) over the energy range under consideration is of the order of ~5–8%. This variation of R_B (and V_B) would correspond to a departure from a $1/E_{c.m.}$ dependence of the fusion cross sections; however, at the present time the accuracy of the data does not allow one to distinguish the small variation with any certainty. In order

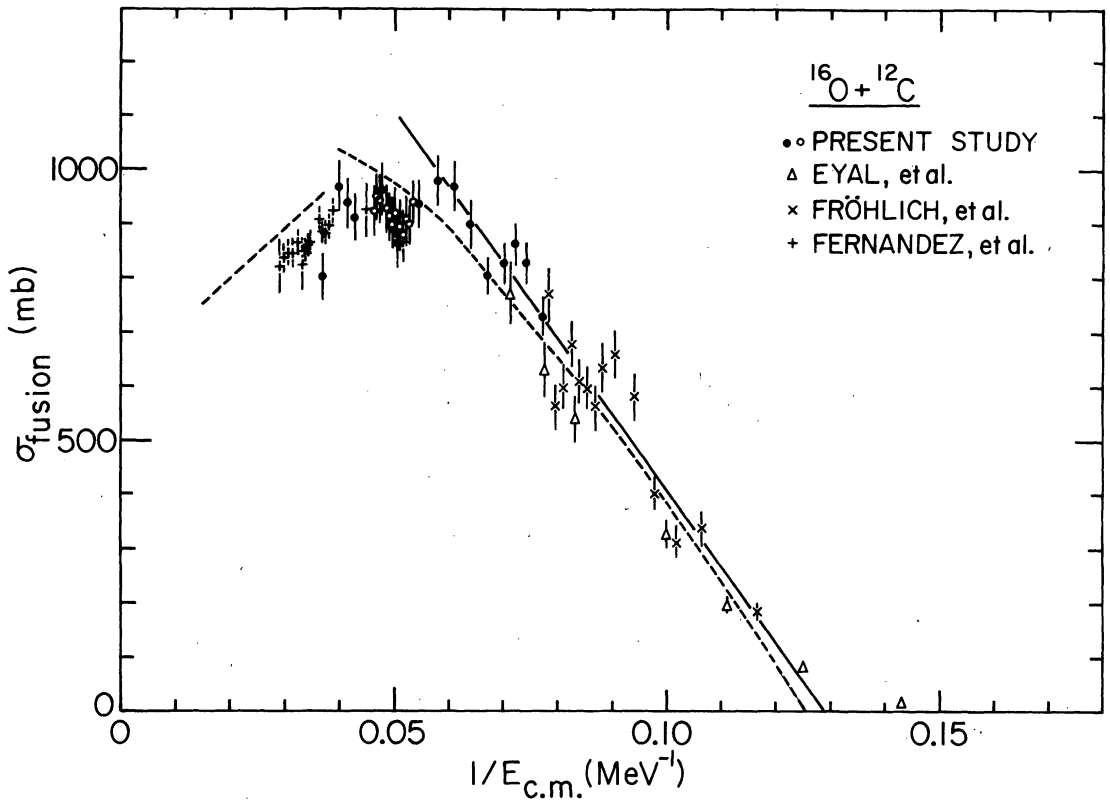

FIG. 13. Total fusion cross sections for the $^{16}O+^{12}C$ system established in this study plotted versus $1/E_{c.m.}$. The solid and open circles represent cross sections established from full angular distribution and single-angle measurements, respectively. Also plotted are the results of Refs. 22–24. (For description of curves, see Fig. 6.)

to predict the energy dependence (or dependence on the angular momentum l) of R_B, a specific potential has to be assumed and a number of approaches for predicting or establishing the properties of the interaction potential are reported in the literature. Recently Bass[41] and Horn and Ferguson,[45] for example, have used the fusion data to establish empirical potentials, while Birkelund *et al.*[46] and Vaz and Alexander,[47] for example, have utilized the proximity potential. In the first subsection, the systematics observed in the barrier parameters R_B and V_B extracted from our data will be discussed; in the following subsection, our data will be compared with the fusion cross sections predicted using various ion-ion potentials.

TABLE VII. Total fusion cross sections obtained for the $^{12}C+^{18}O$ system. The underlined energies indicate that full distributions were measured. Optical model parameters of Ref. 7 were used in normalizing the fusion data to elastic scattering.

$E_{c.m.}$ (MeV)	σ_{fus} (mb)	$\Delta\sigma_{fus}$ [a] (mb)
11.94	714	±11
13.94	902	18
14.95	949	19
15.95	1017	18
17.95	1108	28
18.95	1160	40
19.95	1195	24
21.96	1178	26
23.96	1143	30
25.96	1122	25
27.97	1102	30

[a] Relative errors are listed; absolute errors are ~5%.

1. Fusion cross section systematics

Assuming the fusion cross section energy dependence of Eq. (1), we have performed linear least-squares fits to the low energy data of each system investigated in this study to determine R_B and V_B; these fits are indicated as solid lines in Figs. 6–8, 10, 13–15, and 17. Only data over the energy range ≈1.1 to ≈2.0 times the Coulomb barrier were used. The barrier parameters, R_B and V_B obtained are listed in Table X. Similar fits were performed for a number of other sys-

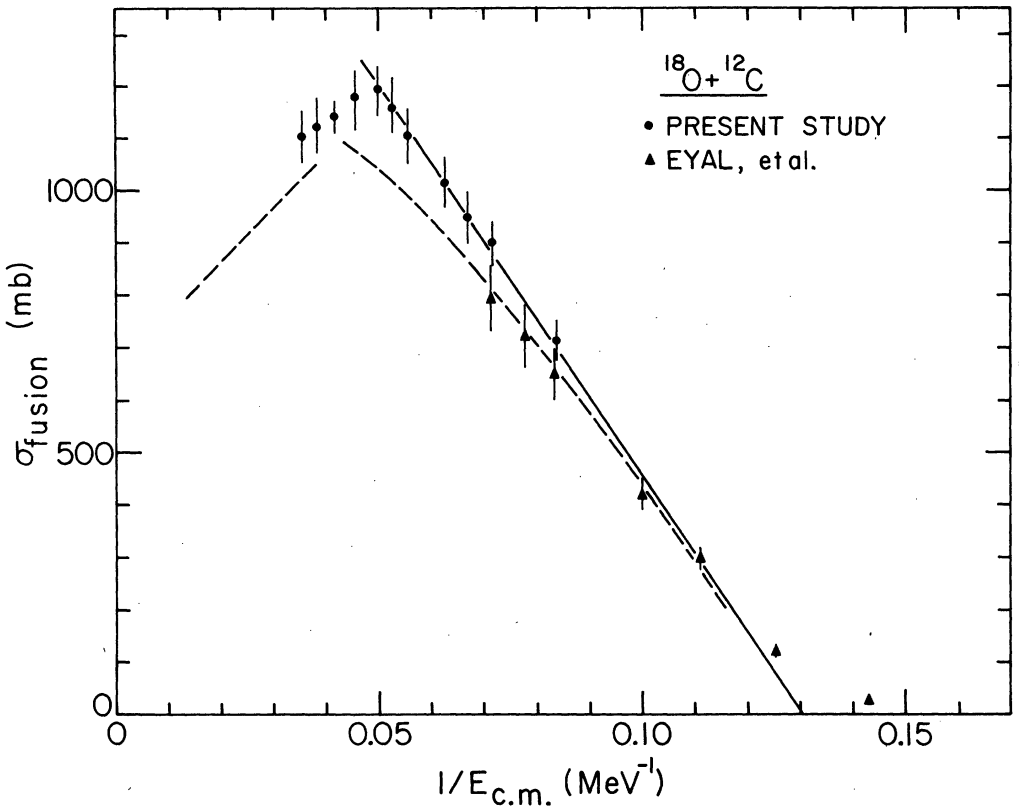

FIG. 14. Total fusion cross sections for the $^{18}O+^{12}C$ system established in this study plotted versus $1/E_{c.m.}$. Also shown are the results of Ref. 22. (For description of curves, see Fig. 6.)

tems reported in the literature, and these parameters are also listed in Table X. These fusion data represent measurements in which different experimental techniques were employed and the emphasis on relative versus absolute cross sections varied. The experimental uncertainties (and in some cases, the significant inconsistencies in overlapping data sets) account for the uncertainties quoted on the barrier parameters.

TABLE VIII. Total fusion cross sections established for the $^{12}C+^{19}F$ system. The underlined energies indicate that full angular distributions were measured. Optical model parameters of Ref. 7 were used in normalizing the fusion data to elastic scattering.

$E_{c.m.}$ (MeV)	σ_{fus} (mb)	$\Delta\sigma_{fus}$[a] (mb)
11.56	552	±17
13.49	738	20
15.43	880	25
17.37	975	30
19.31	1072	35
21.25	1095	35
23.18	1151	40
25.12	1172	40
27.06	1092	45

[a] Relative errors are listed; absolute errors are 5%.

The barrier parameters obtained for the systems of this study are plotted versus $A_1^{1/3}+A_2^{1/3}$ in Fig. 18, while in Fig. 19, they are plotted together with those extracted for the other systems. There are several interesting features to be noted: (1) For the systems studied here (Fig. 18), the barrier parameters vary rather smoothly; deviations from a smooth behavior are within the uncertainties in the extracted parameters. The deviations seen for some heavier systems (Fig. 19) are somewhat more pronounced. One might have expected that the detailed shapes of the nuclear potentials would manifest themselves in variations of the barrier radii rather than in the values of the barrier height.[57] It is observed, however, that the barrier radii change more smoothly from system to system than do the barrier heights. (2) The dashed lines in Fig. 19 are drawn to represent the average trends of the data. The A dependence of R_B appears to differ considerably be-

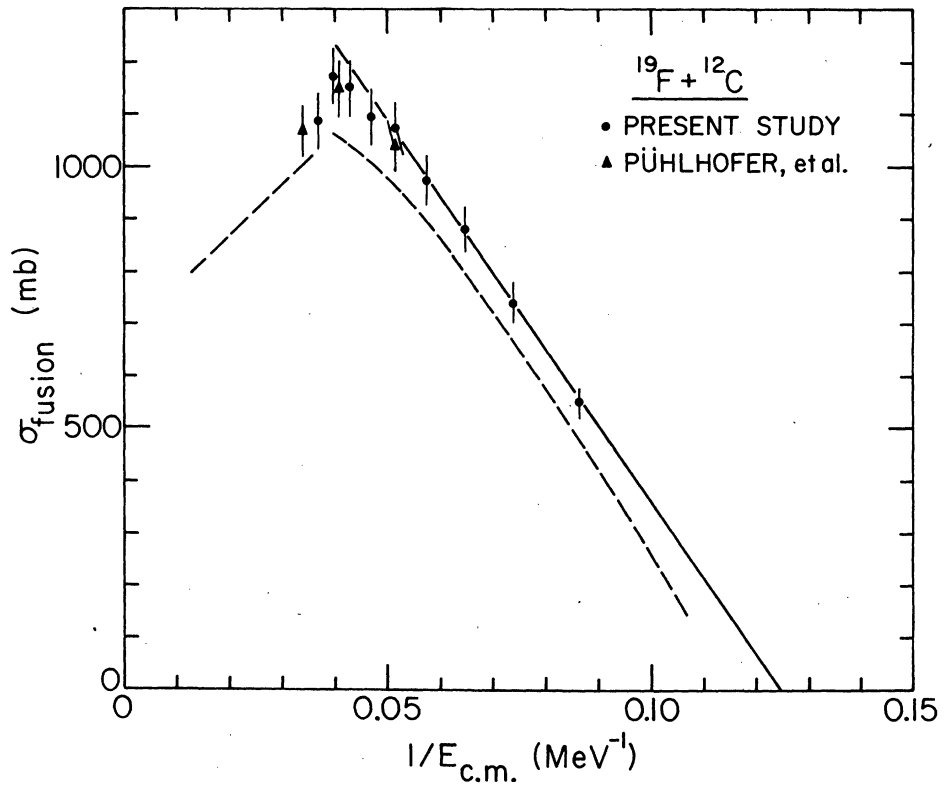

FIG. 15. Total fusion cross sections for the $^{19}F+^{12}C$ system established in this study plotted versus $1/E_{c.m.}$. Also shown are the results of Ref. 33. (For description of curves, see Fig. 6.)

tween the lighter systems and the heavier systems. In particular, the $^{18}O+^{12}C$ and $^{19}F+^{12}C$ systems seem to mark a transition point between the two systematic trends in the barrier radii. It should be noted that little weight should be attached to the choice of $A_1^{1/3}+A_2^{1/3}$ as the ordinate in Figs. 18 and 19. Quite similar systematic trends are observed if, for example, the data for any single projectile are plotted as a function of A_2. (3) Any change in the A dependence of the barrier heights, V_B, in going from the lighter to the heavier systems is much less noticeable. The values for the p-shell systems are very nearly constant as a function of $A_1^{1/3}+A_2^{1/3}$.

2. *Macroscopic models*

Several models have been presented in the literature to calculate fusion barriers. For example, Krappe and Nix,[58] using the liquid-drop model, parametrize the barrier by

$$V_B=\frac{Z_1Z_2e^2}{r_0(A_1^{1/3}+A_2^{1/3})+a+d}, \tag{2}$$

where a is the range of the nuclear potential and d is the distance between surfaces at the barrier; d is determined for each system by iterating the expression for the Coulomb plus liquid drop nuclear potential to find the maximum. The solid curves on Figs. 18 and 19 illustrate these results. For heavy systems, this model works reasonably well; however, it does not account for the A dependence of the barrier radii for the light systems.

As discussed before, the assumption that R_B and V_B are independent of energy, is very convenient; however, it is clear that for any nuclear potential with finite diffuseness, both barrier parameters must be energy dependent. Bass has used the experimental energy dependence of the fusion cross sections to map out a portion of the ion-ion potential for several systems.[41] He then fits these potentials with a single universal interaction obtaining

$$V_{NUC}(s)=\frac{-R_1R_2}{R_1+R_2}\,[0.0300\exp(s/3.3)+0.0061\exp(s/0.65)]^{-1}, \tag{3}$$

where

$$s=r-R_1-R_2 \tag{4}$$

and

TABLE IX. Total fusion cross sections established for the $^{16}O+^{16}O$ and $^{16}O+^{27}Al$ systems in this study. The underlined energies correspond to the energies at which full angular distributions were measured; at other energies the cross sections are based on single-angle ($\theta_{lab}=8°$) measurements. Optical model parameters of Refs. 8 and 9 were used in normalizing total fusion cross sections. See the text for discussion of the errors and the procedure for establishing absolute cross sections.

$E_{c.m.}$ (MeV)	σ_{fus} (mb)	$\Delta\sigma_{rel}$ (mb)	$\Delta\sigma_{abs}$ (mb)
14.92	435	±25	±30
15.92	561	30	50
16.92	604	30	60
17.93	654	35	60
18.93	735	40	70
19.93	785	50	40
20.46	781	45	75
20.93	887	55	75
21.46	936	55	80
21.93	950	60	80
22.47	979	55	80
22.94	937	55	80
23.47	1012	60	80
23.94	845	50	80
24.47	850	50	75
24.94	905	55	80
25.94	890	55	60
26.94	880	50	80
27.94	860	45	80
28.95	930	55	80
29.47	844	50	80
29.95	850	50	60
30.47	919	55	80
30.95	946	55	80
31.47	883	50	80
35.96	905	60	80
	$^{16}O+^{27}Al$		
18.74	351		50
25.03	797		60
32.57	1036		60
37.60	1095		70

$$R_{1(\text{or }2)}=1.16\,A_{1(\text{or }2)}^{1/3}-1.39\,A_{1(\text{or }2)}^{-1/3}. \quad (5)$$

The fusion cross sections calculated with this potential are shown as dashed curves in Figs. 6, 8, 10, 13–15, and 17. As can be seen, the Bass potential overestimates the strength for the $^{12}C+^{12}C$ and $^{16}O+^{16}O$ systems, approximately reproduces the behavior for the $^{12}C+^{13}C$, $^{14}N+^{12}C$, $^{15}N+^{12}C$, and $^{16}O+^{12}C$ systems, and underestimates the strength for the $^{18}O+^{12}C$ and $^{19}F+^{12}C$ systems. The question of whether the observed disagreement in fact reflects a structure dependence of the interaction barrier remains to be answered.

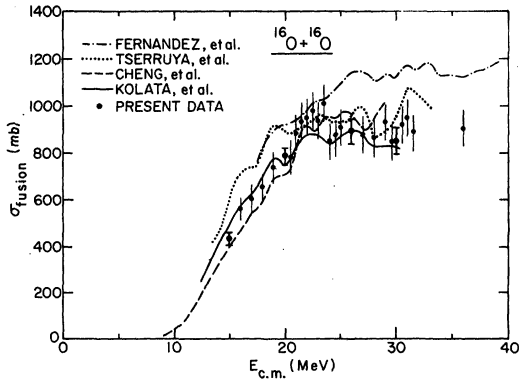

FIG. 16. Fusion cross sections for the $^{16}O+^{16}O$ system plotted versus $E_{c.m.}$. The curves shown represent the behavior of the fusion cross sections observed in the studies of Refs. 24, 36–38.

For the range of $\sigma_{fus}(E)$ from 200 mb to 800 mb, $R_B(E)$ as predicted by the Bass potential changes roughly by 8–10% for the systems considered. The use of the Bass potential for the higher energy data will be discussed in the next subsection.

Recently Horn and Ferguson[45] presented a parametrization for fusion cross sections which involves two terms; one characterizing the compound nucleus and one the entrance channel. This parametrization is of the form:

$$\sigma_{fus}(E)=\pi\rho^2\left(1-\frac{D}{\rho}\right), \quad (6)$$

where the collision distance $D=Z_1Z_2e^2/E$. The parameter ρ is taken in place of the fixed distance R_B of Eq. (1). Based on fits to fusion data, a linear relationship for ρ with energy is observed, i.e.,

$$\rho=mE+b, \quad (7)$$

where b was taken to be the sum of the radii at 1.35% of the central charge density for target and projectile, and m was found to be

$$m^{-1}=18(2.23-A_{cn}^{1/3}), \quad (8)$$

where A_{cn} is the mass of the compound nucleus. They reproduced the behavior of the fusion cross section over the energy range ≈1.2 to ≈2.0 times the Coulomb barrier energy for systems spanning the mass range from $^{12}C+^{14}N$ to $^{35}Cl+^{124}Sn$. We compared the predictions of Eq. (6) to the fusion cross sections observed for the systems of this study. The quality of the fits was similar to that observed for the Bass predictions. While rather acceptable agreement was observed for a number systems, poor agreement was observed for the $^{12}C+^{13}C$ and $^{16}O+^{16}O$ systems, for example, with

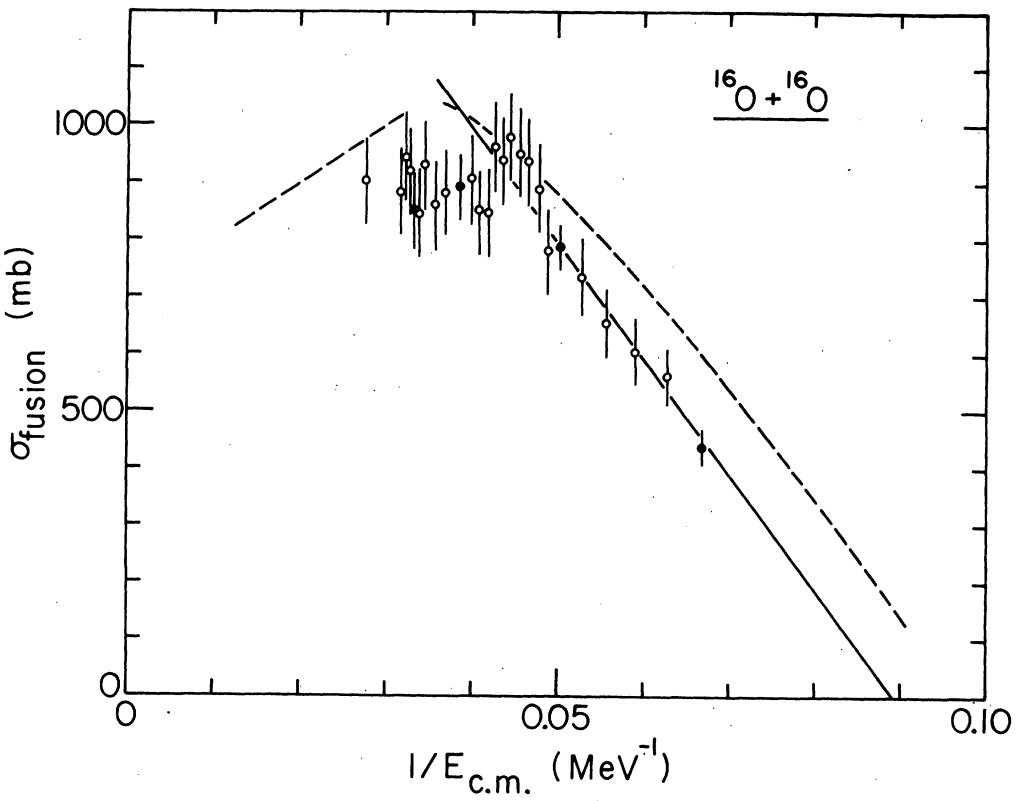

FIG. 17. Total fusion cross sections for the $^{16}O+^{16}O$ system established in this study plotted versus $1/E_{c.m.}$. The solid and open circles represent cross sections established from full angular distribution and single-angle measurements, respectively. (For description of curves, see Fig. 6.)

discrepancies of the order of 100 mb.

Recently two analyses using the proximity potential have been presented. In the work of Birkelund *et al.*,[46] a model based on the proximity potential with one-body friction has been proposed. In the energy range under consideration, this model reproduces the data observed for heavier systems; however, predictions for systems as light as ours have not been presented thus far. In the work of Vaz and Alexander,[47] systematics of fusion barriers obtained using a modified proximity potential are presented for systems $30 \lesssim Z_1 Z_2 \lesssim 1500$. Barrier penetration as well as the l dependence of the fusion radius are included. The general form of the proximity potential is assumed with small, but important, parameter adjustments made to achieve a fit to the experimental data. In the fitting procedure, a single parameter ΔR [which modifies the recommended value of the radius parameter for the proximity potential $V_M(r)$] is varied. As found by Vaz and Alexander, the fitting parameters ΔR for the various systems show a systematic trend, but scatter wildly around the mean value by ~0.1 fm. The fluctuations in ΔR appear to be outside the random errors and may well reflect the individual shell structures and deformations of the collision partners. These results are very suggestive and indicate that this approach is perhaps promising for quantitatively establishing the influence of structure on the fusion cross sections in this energy range.

C. Limitation of fusion cross section

1. Cross section systematics

At "higher" energies, corresponding to roughly twice the Coulomb barrier and above, the fusion cross sections are observed to change less rapidly with increasing bombarding energy. For light systems such as considered here, the cross sections appear to decrease or remain roughly constant, while for heavier systems, the cross sections still increase but much more slowly than the total reaction cross sections. Measurements[39] on heavier systems have shown that the fusion cross sections vary approximately linearly with $1/E_{c.m.}$ and can be parametrized in a fashion identical to Eq. (1); i.e.,

TABLE X. List of the fusion barrier parameters R_B and V_B obtained in fits of Eq. (1) to fusion cross sections. The data used in extracting the parameters are referenced in the last column.

System	R_B	V_B	References
$^{12}C+^{10}B$	5.9 ±0.3	4.8±0.1	48,49
$^{12}C+^{11}B$	6.1 ±0.3	4.8±0.1	48
$^{12}C+^{12}C$	6.5 ±0.4	5.8±0.3	present, 12
$^{12}C+^{13}C$	7.0 ±0.2	5.7±0.3	present
$^{12}C+^{14}N$	7.0 ±0.3	6.8±0.2	present, 10,15,17,18
$^{12}C+^{15}N$	7.2 ±0.3	6.3±0.4	present, 15
$^{12}C+^{16}O$	7.5 ±0.3	7.7±0.4	present, 22, 23, 24
$^{12}C+^{17}O$	7.3 ±0.3	7.7±0.6	22
$^{12}C+^{18}O$	7.9 ±0.3	7.7±0.2	present, 22
$^{12}C+^{19}F$	7.6 ±0.2	8.0±0.4	present
$^{14}N+^{14}N$	7.2 ±0.4	7.9±0.6	16
$^{16}O+^{16}O$	7.6 ±0.4	11.2±0.6	present
$^{16}O+^{24}Mg$	8.4 ±0.4	15.9±0.9	50
$^{16}O+^{26}Mg$	8.7 ±0.4	16.5±0.9	50
$^{16}O+^{27}Al$	8.1 ±0.3	15.7±0.5	34,35
$^{16}O+^{40}Ca$	9.0 ±0.4	23.7±1.0	51,52
$^{17}O+^{27}Al$	8.5 ±0.3	15.8±0.6	34
$^{18}O+^{24}Mg$	7.8 ±0.3	14.9±0.9	50
$^{18}O+^{27}Al$	8.29±0.3	15.6±0.6	34
$^{32}S+^{24}Mg$	8.7 ±0.3	28.1±1.6	44,53
$^{32}S+^{40}Ca$	9.0 ±0.7	43.3±4.5	44
$^{35}Cl+^{27}Al$	8.8 ±0.4	32.0±2.6	55
$^{35}Cl+^{48}Ti$	8.7 ±0.4	49.2±3.8	55
$^{35}Cl+^{56}Fe$	9.7 ±0.8	55.1±5.0	55
$^{35}Cl+^{58}Ni$	9.2 ±0.4	61.8±3.5	55,56
$^{35}Cl+^{60}Ni$	9.0 ±1.2	60.5±3.6	56
$^{35}Cl+^{62}Ni$	9.5 ±0.4	60.6±3.9	55,56
$^{35}Cl+^{64}Ni$	9.5 ±0.4	60.0±4.1	55,56
$^{35}Cl+^{90}Zr$	9.7 ±0.4	83.9±3.5	55
$^{40}Ca+^{40}Ca$	9.5 ±0.5	50.6±2.8	54

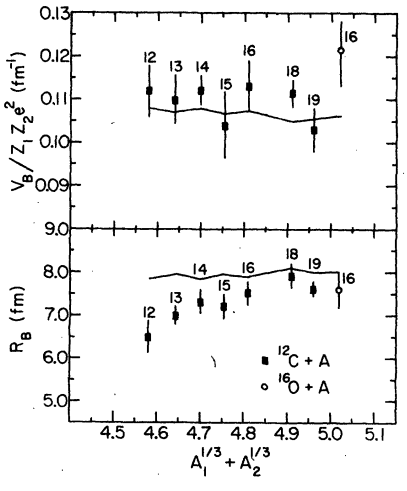

FIG. 18. The barrier parameters R_B and V_B (i.e., $V_B/Z_1Z_2e^2$) extracted from fits to the fusion data of this study plotted versus $(A_1^{1/3}+A_2^{1/3})$. The curves shown are discussed in the text.

$$\sigma_{fus}(E)=\pi R_{cri}^2\left(1-\frac{V_{cri}}{E_{c.m.}}\right), \tag{9}$$

where R_{cri} is interpreted as the minimum radius which the nuclei must reach to fuse and V_{cri} as the value of the total (nuclear plus Coulomb) potential at this radius. In these studies[39] the data were found to be consistent with $R_{cri}=r_{cri}(A_1^{1/3}+A_2^{1/3})$, where $r_{cri}=1.0\pm0.07$ fm and $V_{cri}=(0.124Z_1Z_2-17.6)$ MeV for $Z_1Z_2<1000$.

In the present study, the high energy data extend over a relatively small range in $1/E_{c.m.}$, and R_{cri} and V_{cri} cannot be independently determined. Even when these data are considered together with other data, little can be learned about the systematics, and even evidence for a $1/E_{c.m.}$ dependence is not conclusive. While higher energy data for the $^{12}C+^{12}C$ system exist, the inconsistencies between our cross sections and those of Namboodiri, Chulick, and Natowitz[12] in the energy range of overlap, make it difficult to draw conclusions. It does appear that σ_{fus} decreases at the highest energies. Similar and indeed more serious discrepancies exist for the $^{16}O+^{16}O$ system as noted previously. For the $^{16}O+^{12}C$ system the data suggest that σ_{fus} decreases at higher energies. It is only for the $^{14}N+^{12}C$ system that high energy data exist and all studies agree in the region of overlap. Stokstad *et al.*[10] quote $R_{cri}=1.08$ fm and $V_{cri}=-2$ MeV based on their fit to the data. Their cross section at the highest energy measured is ≈200 mb smaller than that observed at slightly lower energies (Fig. 8), and has been interpreted as evidence for a liquid-drop limitation on σ_{fus}.[10,59]

The one quantity which does appear to be somewhat better determined for light systems at the higher energies is the value of the maximum fusion cross section, σ_{fus}^{max}. The values of σ_{fus}^{max} established in our measurements together with those reported in the literature for other systems[35,50,51,60] involving ^{12}C and ^{16}O ions are shown in Fig. 20. With the exception of one system ($^{15}N+^{12}C$), there appears to be a rather striking difference, depending on whether both ions have nucleons occupying only the $1p$ shell or whether one of them also has some occupation of the s-d shell; σ_{fus}^{max} in the former case being ≈950 mb, while σ_{fus}^{max} in the latter case is ≈1200 mb. The glaring exception to the trend is the $^{15}N+^{12}C$ system with a maximum fusion cross section of 1180 mb. Preliminary results of other exceptions to this trend have been reported[61] and the final results of these measurements are of great interest. We showed in the previous section that the barrier radii for the s-d shell systems fall on a smooth extrapolation from the lighter p-shell system. Such an ef-

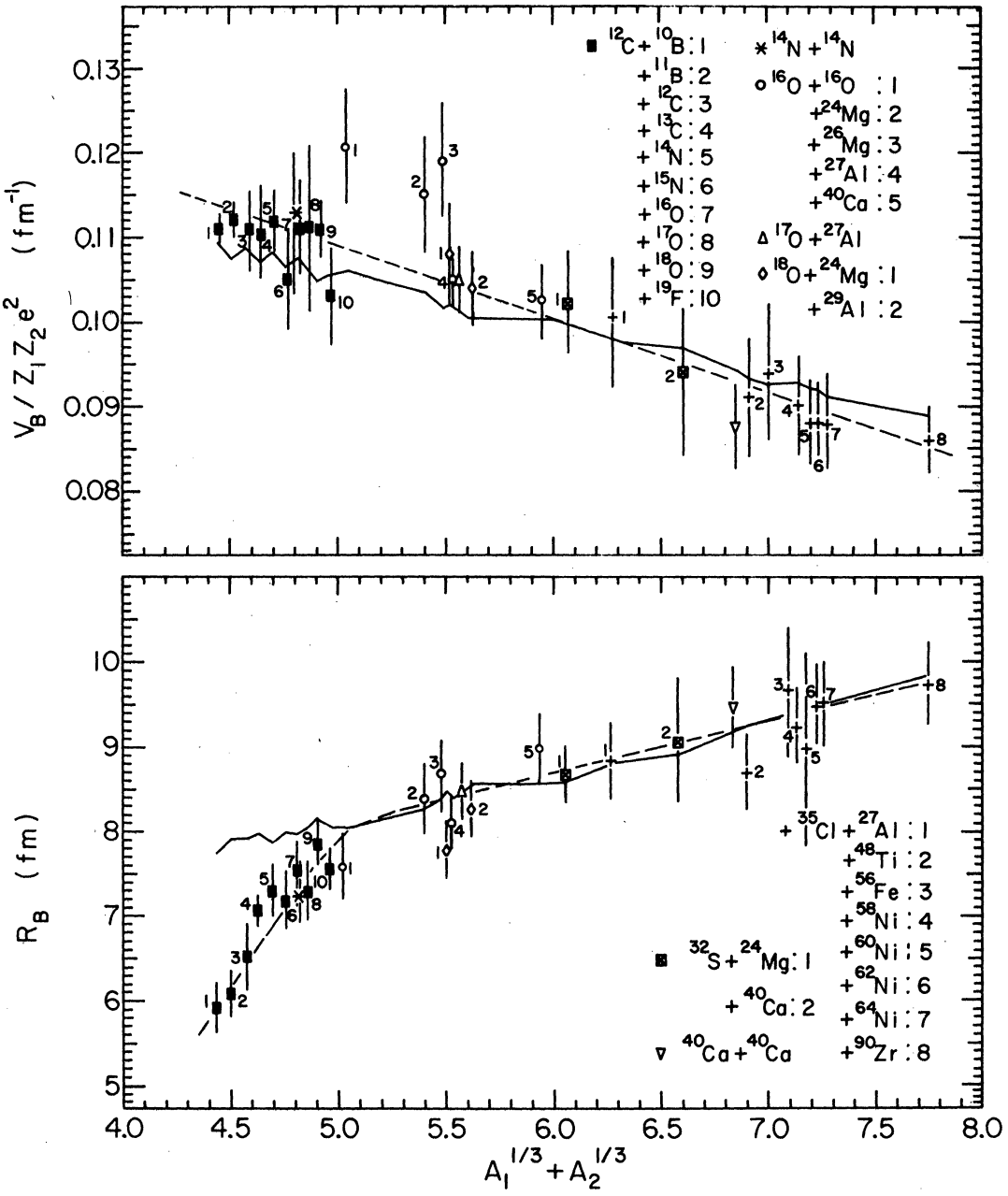

FIG. 19. The barrier parameters R_B and V_B (i.e., $V_B/Z_1Z_2e^2$) listed in Table X plotted versus $(A_1^{1/3}+A_2^{1/3})$. The definition of the symbols are spread between the two parts of the figure. The solid curves shown are discussed in the text. The dashed curves indicate the average trends. The A dependence of R_B can be approximated by two linear segments; i.e., R_B (fm) $= -10.50 + 3.71\ [A_1^{1/3}+A_2^{1/3}]$ for $A_1^{1/3}+A_2^{1/3} < 5.0$ and R_B (fm) $= 5.06 + 0.61\ [A_1^{1/3}+A_2^{1/3}]$ for $A_1^{1/3}+A_2^{1/3} \geq 5.0$. The barrier height has the dependence $V_B/V_1Z_2e^2 \cong 0.153 - 0.00875\ [A_1^{1/3}+A_2^{1/3}]$.

fect must be intimately connected with the limiting mechanism, and so may lead to a clue regarding the underlying reaction process.

2. *Model discussion*

(*a*) *Entrance channel effects.* As noted at the beginning of this section, possible explanations of the $\sigma_{fus}(E)$ behavior in this energy region have fallen into two categories, i.e., entrance channel effects, or properties of the compound nucleus. In entrance channel models, the behavior of the fusion process is understood as resulting from an

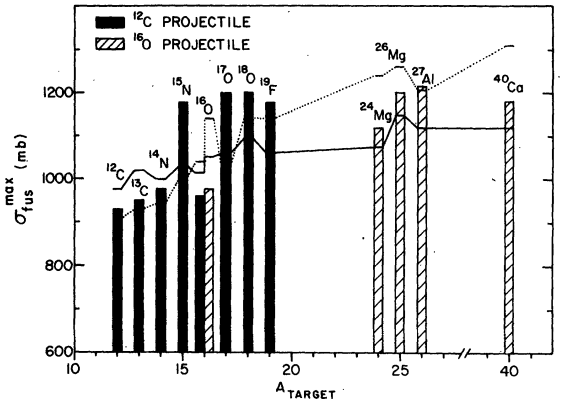

FIG. 20. Plot of σ_{fus}^{max} observed for a number of systems involving ^{12}C and ^{16}O ions on targets in the $1p$ and $2s1d$ shell. These values are from the present study and the studies of Refs. 35, 50–52, 60. The solid and dotted lines represent σ_{fus}^{max} predictions of the Bass model and the Horn and Ferguson model, respectively (see text).

interplay between dissipative and conservative forces. Friction between the two ions converts energy (angular momentum) of relative motion into intrinsic excitation and thus may cause trapping of the two ions in the ion-ion potential well. The simplest model, first suggested by Galin *et al.*,[39] makes the assumption that strong friction sets in only at a "critical" radius, R_{cri}, thus trapping all the ions that reach this point. Fits to fusion data using Eq. (9) give values of R_{cri} which are very nearly equal to the sum of two half-density radii, consistent with the distance where major rearrangements of nuclear structure and the corresponding energy losses are expected to take place.[62] In this picture, the concept of a R_{cri} is valid over the entire energy range; at low energies the fusion cross section is determined by the interaction barrier [Eq. (1)] that must be overcome to reach R_{cri}, and at higher energies the fusion cross section is determined by the highest partial wave which reaches R_{cri} [Eq. (9)].

If the Bass potential is assumed and R_{cri} is taken to be $R_{cri}=R_1+R_2$ [from Eq. (5)], one finds that the predicted cross sections rather poorly reproduce the high energy experimental data and, in particular, they do not reproduce the differences in σ_{fus}^{max} between neighboring systems. These predictions are shown on Figs. 6–8, 10, 13–15, and 17 as dashed curves. The values of σ_{fus}^{max} as determined from the intersections of the low energy and high energy predictions are shown in Fig. 20 as the solid line. It should be noted that in the recent Birkelund *et al.*[46] study, in which a frictional force was employed, it was shown the predicted σ_{fus}^{max} and the slope of $\sigma_{fus}(E)$ at higher energies differed significantly from those predicted in friction-free calculations. While this may imply some changes for light systems such as studied here, it is unlikely to explain the abrupt changes in σ_{fus}^{max} as seen for ^{14}N+^{12}C and ^{15}N+^{12}C, for example.

In the work of Horn and Ferguson,[45] discussed previously, it was suggested that the abrupt changes in σ_{fus}^{max} might follow naturally from the parametrization of the radius dependence for a specific density overlap (i.e., 1.35% of central density) of target and projectile. When this prescription is used for the systems sutdied here, we find that the predicted σ_{fus}^{max} depends sensitively on what nuclear charge-density distribution is used; the values of σ_{fus}^{max} can vary by as much as 10% depending on what parameters are chosen from the literature. Using the most recent experimental results quoted in de Jager, H. de Vries, and C. de Vries[63], we have calculated $\sigma_{fus}(E)$ for the systems studied here, as well as for some other ^{16}O-induced reactions on heavier targets. In Fig. 20, the predicted σ_{fus}^{max} are shown by the dotted line and compared with those observed experimentally. As can be seen, discrepancies on the order of $\gtrsim 100$ mb are seen.

In all the explanations given, it is always assumed that the limitation on σ_{fus} is imposed by the failure of the largest partial waves to contribute to fusion. Recently, time dependent Hartree Fock (TDHF) calculations have suggested that it is the lower partial waves which do not fuse and that the limitation to fusion is imposed by a low-l cutoff (e.g., Ref. 64 and 65). Calculations have been performed by Flocard, Koonin, and Weiss[64] for the ^{16}O+^{16}O system. In this system, there are large discrepancies in the data; while the predicted fusion cross sections in this high energy region are ≈300 mb larger than observed in the present study, they are in rather good agreement with those of Ref. 23. A low-l cutoff may manifest itself in the distribution of strength in the evaporation residues. Such a distribution of strength was not measured for the ^{16}O+^{16}O system in the present study.

(*b*) *Yrast-spin limitation.* As suggested by Harar,[15] the limitation of $\sigma_{fus}(E)$ at higher energies could be due to an angular momentum limitation imposed by the properties of the compound nucleus. Specifically, if at a given excitation energy in the compound nucleus, the grazing angular momentum l_{gr} is larger than the yrast-spin at this excitation, then the compound nucleus cannot accommodate all the angular momentum brought into it. The yrast band in the compound nucleus can be described by

$$E_J = E_0 + \frac{\hbar^2}{2\mathcal{I}} J(J+1), \tag{10}$$

where E_0 is the band head excitation energy, $\mathcal{I}$ is the moment of inertia, and E_J is the excitation energy of the yrast state of angular momentum J. Then assuming $l_{cri} = J$, the fusion cross sections can then be written as

$$\sigma_{fus}(E_{c.m.}) \leq \pi\lambda^2(J+1)^2 \approx \frac{\pi\mathcal{I}}{\mu}\left(1 - \frac{E_0 - Q}{E_{c.m.}}\right), \qquad (11)$$

where Q is the ground state Q value for the fusion reaction. As can be seen, this equation is identical in form to Eq. (9) which is not surprising since the semiclassical models used imply a direct correspondence between a critical angular momentum and a critical distance.

If the moments of inertia and band head energies were roughly constant throughout the compound nuclei in the upper s-d shell, then the apparent shell effect in σ_{fus}^{max} might simply be a result of the Q values for the $^{19}F + ^{12}C \rightarrow ^{31}P$ and $^{18}O + ^{12}C \rightarrow ^{30}Si$ reactions being ≈25% larger than for the other reactions. Such an explanation has been proposed by Harar[15] for the difference in σ_{fus}^{max} for the $^{14}N + ^{12}C$ and $^{15}N + ^{12}C$ systems, where Eq. (11) predicts a ≈10% larger strength for the $^{15}N + ^{12}C$ system. However, recently Mosel[43] has addressed this question more quantitatively. First, Mosel argues that for the systems considered ($^{12}C + ^{12}C$, $^{12}C + ^{14}N$, $^{12}C + ^{16}O$, $^{12}C + ^{18}O$, and $^{12}C + ^{19}F$), the experimental excitations in the compound nuclei are considerably above the expected yrast lines. For all but the $^{12}C + ^{12}C$ and $^{12}C + ^{14}N$ systems, a limitation due to the yrast band can be ruled out; but even for these two systems, when deformation and shell effects were included in determining the yrast line, it was concluded that such a limitation cannot be responsible for the observed drop of σ_{fus} below σ_{react} at the higher energies.

D. Systems with oscillatory structure

One of the most interesting results of this study of fusion cross sections of p-shell nuclei was the observation of oscillatory structure in the energy dependence of the fusion cross sections for three systems: $^{12}C + ^{12}C$, $^{16}O + ^{12}C$, and $^{16}O + ^{16}O$. Since the initial report of this effect,[1] many other groups have studied one or more of these reactions by a variety of techniques. The common results seem to be the following: (1) In γ-ray measurements which can identify the final residual nucleus, in α-particle yield measurements, and in measurements of the elemental evaporation residue yields, the structure is found to occur primarily in the α-emission channels. It is not yet entirely clear whether this is the case only because α emission is the favored decay mode of high angular momentum states, or whether nuclear structure effects are responsible. Evaporation calculations indicate that of those compound nuclei formed by the largest partial wave contributing to fusion, approximately 90% decay by α emission. (2) Similar gross structure resonances have been observed in some inelastic and transfer reactions for these systems; i.e., $^{12}C(^{12}C, ^{12}C)^{12}C(2^+)$, $^{12}C(^{16}O, ^{16}O)^{12}C(2^+)$, and $^{16}O(^{16}O, ^{12}C)^{20}Ne_{g.s.}$.[66-68] Cormier *et al.*[66] have assigned spins which are near the grazing partial waves to these structures by, somewhat arbitrarily, identifying the spins of these gross structure resonances with those of known narrower (intermediate structure) resonances in the same energy region. (3) Calculations of the total reaction cross sections for the $^{12}C + ^{12}C$ and $^{16}O + ^{16}O$ systems with optical potentials which are fit to the elastic scattering show structures which are qualitatively similar to those observed in the fusion cross sections. These potentials are all weakly absorbing at the nuclear surface.[6,8] For $^{16}O + ^{12}C$, it is necessary to decrease the absorption of the potential of Ref. 7 to obtain such structures in the total reaction cross sections. (4) The addition of one or more particles to either of the ions in the entrance channel reduces any structure considerably; i.e., the measured fusion cross sections are somewhat larger and within statistics vary much more smoothly with energy.

Since weak absorption is crucial for the observation of shape resonances, the addition of one or more nucleons may provide a damping mechanism to broaden the widths of the resonance structure. The three systems showing structure in fusion all possess rather special symmetries; $^{12}C + ^{12}C$ and $^{16}O + ^{16}O$ are identical particle systems and $^{16}O + ^{12}C$ is related to $^{12}C + ^{12}C$ by α-particle exchange. For the identical particle systems, odd partial waves are forbidden, and the relative spacing of single particle resonances is thus greater than for nonidentical systems. In fact, the calculated total reaction cross section for nonidentical mass-12 particles with the $^{12}C + ^{12}C$ potential of Ref. 6 does not show structure. α-exchange effects could introduce a situation in the $^{12}C + ^{16}O$ system where the even partial waves are responsible for the observed structures. Comparison of the structures observed in the calculated reaction cross section for the $^{16}O + ^{16}O$ system to those observed in the experimental fusion cross sections shows that the spacing of the structures are in good agreement. For the $^{12}C + ^{12}C$ system, the spacings of the structures in the predicted reaction cross sections and in the observed fusion cross sections are similar but are out of phase. Calculations including single and double excitation of $^{12}C(2^+)$ have shown that this might be understood as resulting

from coupled-channel effects.[69] Hence, at this time, the "gross" structures observed in the fusion data appear to be associated with the shape resonances in the entrance channel. To date, no measurements of fusion cross sections for other light identical particle systems have been performed in the energy range considered here.

V. CONCLUSIONS

In this paper, we have reported a large body of measurements of fusion cross sections for target and projectile systems with $12 \leq A \leq 19$. In these reactions, the fusion component is the largest single part of the total reaction cross section, and an understanding of the fusion mechanism is crucial to a description of the complete target-projectile interaction. The three primary results which have been obtained are the following: (1) Structures are observed in the energy dependence of the total fusion cross sections for $^{12}C+^{12}C$, $^{16}O+^{12}C$, and $^{16}O+^{16}O$. (2) In the energy region dominated by the interaction barrier, the A dependence of the barrier radii for the systems studied here does not follow the same general systematics as for the heavier systems. The $^{19}F+^{12}C$ and $^{18}O+^{12}C$ systems seem to mark a transition point between the two systematic trends. (3) At higher energies, the maximum fusion cross sections appear to be either $\approx$950 mb or $\approx$1200 mb. Most puzzling at this time is the sudden change in σ_{fus}^{max} for systems differing by a nucleon or two (e.g., $^{12}C+^{14}N$ and $^{12}C+^{15}N$, and $^{12}C+^{16}O$ and $^{12}C+^{17,18}O$). Our results have been viewed in the context of other results in order to attempt to establish the systematic behavior and have been discussed in the framework of macroscopic models. In this framework, it is concluded that while the low-energy, barrier dominated, fusion cross section behavior does not show a strong sensitivity to the details of the entrance channel, nuclear structure effects must be important in the limitation of the fusion cross sections at high energies. To reveal the dependence on nuclear structure at the lower energies, more detailed data which better define the distribution of reaction strength and more sophisticated models to describe the reaction process appear to be necessary.

ACKNOWLEDGMENTS

The authors wish to express their thanks to the tandem operating staff for their efforts and cooperation. Thanks are also extended to K. Daneshvar for his work on the ΔE-E gas ionization detector used in the measurements. C. Olmer's comments on the manuscript are also gratefully acknowledged. This work was performed under the auspices of the U. S. Department of Energy. K. E. Rehm was supported in part by a Max Kaole fellowship.

---

*Present address: Israel Atomic Energy Commission, Soreq Nuclear Research Center, Yavne, Israel.
†Present address: Department of Nuclear Physics, Australian National University, Canberra, Australia.
‡Present address: Technische Universität München, D-8046 Garching, W. Germany.
§Present address: Physik-Department, Technische Universität München, D-8046 Garching, W. Germany.
||Present address: Department of Physics and Astronomy, University of Maryland, College Park, Maryland 20742.
¶Present address: Department of Physics, Indiana University, Bloomington, Indiana 47401.

[1]P. Sperr, S. E. Vigdor, Y. Eisen, W. Henning, D. G. Kovar, T. R. Ophel, and B. Zeidman, Phys. Rev. Lett. 36, 405 (1976).
[2]P. Sperr, T. H. Braid, Y. Eisen, D. G. Kovar, F. W. Prosser, Jr., J. P. Schiffer, S. L. Tabor, and S. E. Vigdor, Phys. Rev. Lett. 37, 321 (1976).
[3]S. Harar, in *Colloque Franco-Japanais de Spectroscopie Nucleaire et Reaction Nucleaire*, Dogashima, Japan, edited by Y. Shida (Institute for Nuclear Study, University of Tokyo, 1976), p. 191.
[4]D. G. Kovar, in *Proceedings of the Symposium on the Macroscopic Features of Heavy Ion Reactions and the Pre-Equilibrium Processes*, Hakone, Japan, edited by H. Kamitsubo and M. Ishihara (Institute of Physical and Chemical Research, Cyclotron Progress Report, Supplement 6, 1977), p. 18; D. G. Kovar, K. Daneshvar, D. F. Geesaman, W. Henning, F. W. Prosser, K. E. Rehm, J. P. Schiffer, and S. L. Tabor, in *Proceedings of the International Conference on Nuclear Structure, Tokyo, 1977*, edited by T. Marumori (Physical Society of Japan, Tokyo, 1978).
[5]M. M. Fowler and R. C. Jarad, Nucl. Instrum. Methods 124, 341 (1975).
[6]D. A. Bromley, in *Nuclear Reactions Induced by Heavy Ions*, edited by R. Bock and W. R. Hering (North-Holland, Amsterdam, 1970).
[7]R. E. Malmin, Argonne National Laboratory, Physics Division Informal Report No. PHY-1972F (unpublished); R. H. Siemssen, in *Proceedings of the Symposium on Heavy Ion Scattering*, Argonne National Laboratory, 1971, edited by R. H. Siemssen (Argonne National Laboratory, Argonne, Illinois, 1971), p. 145.
[8]J. V. Maher, M. W. Sachs, R. H. Siemssen, A. Weidinger, and D. A. Bromley, Phys. Rev. 188, 1665 (1969).
[9]A. Gobbi, R. Wieland, L. Chua, D. Shapira, and D. A. Bromley, Phys. Rev. C 7, 30 (1973).
[10]R. G. Stokstad, R. A. Dayras, J. Gomez del Campo, P. H. Stelson, C. Olmer, and M. S. Zisman, Phys. Rev. Lett. 70B, 289 (1977); R. G. Stokstad, J. Gomez, del Campo, J. M. Biggerstaff, A. H. Snell, and P. H. Stelson, *ibid.* 36, 1529 (1976).

[11]J. J. Kolata, R. M. Freeman, F. Haas, B. Hersch, and J. Gallman, Phys. Lett. 65B, 333 (1976).
[12]M. N. Namboodiri, E. T. Chulick, and J. B. Natowitz, Nucl. Phys. A263, 491 (1976).
[13]H. Spinka and H. Winkler, Nucl. Phys. A232, 456 (1974).
[14]K. A. Erb, R. R. Betts, and D. A. Bromley, in *Proceedings of the International Conference Structure, Tokyo, 1977,* edited by T. Marumori (Physical Society of Japan, Tokyo, 1978), p. 640.
[15]M. Conjeaud, S. Gary, S. Harar, and J. P. Wieleczko, Nucl. Phys. A309, 515 (1978); S. Harar, in *Nuclear Molecular Phenomena*, edited by M. Cindro (North-Holland, Amsterdam, 1978), p. 329.
[16]R. A. Daryas, R. G. Stokstad, Z. E. Switkowski, and R. M. Wieland, Nucl. Phys. A265, 153 (1976).
[17]Z. E. Switkowski, R. G. Stokstad, and R. M. Wieland, Nucl. Phys. A279, 502 (1977).
[18]J. A. Kuehner and E. Almqvist, Phys. Rev. 134, B1229 (1964).
[19]E. Almqvist, D. A. Bromley, and J. A. Kuehner, in *Proceedings of the Second Conference on Reactions between Complex Nuclei, Gatlinburg, Tennessee,* edited by A. Zucker, F. T. Howard, and E. C. Halbert (Wiley, New York, 1960), p. 282.
[20]S. L. Tabor, Y. Eisen, D. G. Kovar, and Z. Vager, Phys. Rev. C 16, 673 (1977).
[21]A. Weidinger, F. Busch, G. Gaul, W. Trautman, and W. Zipper, Nucl. Phys. A263, 511 (1976).
[22]Y. Eyal, M. Beckman, R. Chechik, Z. Frankel, and H. Stocker, Phys. Rev. C 13, 1527 (1976).
[23]H. Fröhlich, P. Dück, W. Galster, W. Treu, H. Voit, H. Witt, W. Kühn, and S. M. Lee, Phys. Lett. 64B, 408 (1976).
[24]B. Fernandez, C. Gaarde, J. S. Larsen, S. Pontoppidan, and F. Videbaek, Nucl. Phys. A306, 259 (1978).
[25]J. R. Patterson, B. N. Magorcka, G. D. Symons, and N. M. Zuk, Nucl. Phys. A165, 545 (1971).
[26]Z. E. Switkowski, R. G. Stokstad, and R. M. Wieland, Nucl. Phys. A274, 202 (1976).
[27]Z. E. Switkowski, H. Winkler, and P. R. Christensen, Phys. Rev. C 15, 449 (1977).
[28]V. Cujec and C. A. Barnes, Nucl. Phys. A266, 461 (1976).
[29]P. R. Christensen, Z. E. Switkowski, and R. A. Dayras, Nucl. Phys. A280, 189 (1977).
[30]D. Branford, B. N. Magorcka, and J. O. Newton, J. Phys. C 3, 1565 (1977).
[31]Y. D. Chan, H. Bohn, R. Vandenbosch, K. G. Berndardt, J. C. Cramer, R. Sielemann, and L. Green, Nucl. Phys. A303, 500 (1978).
[32]V. K. C. Cheng, D. L. Clark, J. R. Han, Y. Mahmud, and S. S. Hanna, Nucl. Phys. (to be published).
[33]F. Pühlhofer, W. Pfeffer, B. Kohlmeyer, and W. F. W. Scheider, Nucl. Phys. A244, 329 (1975).
[34]Y. Eisen, I. Tserruya, Y. Eyal, Z. Frankel, and M. Hillmann, Nucl. Phys. A291, 459 (1977).
[35]B. B. Bock, R. R. Betts, C. Gaarde, J. S. Larsen, E. Michelsen, and Tai Kuang-Shi, Nucl. Phys. A283, 317 (1977).
[36]I. Tserruya, Y. Eisen, D. Pelte, A. Gavron, H. Oeschler, D. Berndt, and H. L. Harney, Phys. Rev. C 18, 1688 (1978).
[37]J. J. Kolata, R. C. Fuller, R. M. Freeman, F. Haas, D. Hensch, and A. Gallmann, Phys. Rev. C 16, 891 (1977).
[38]V. K. C. Cheng, A. Little, H. C. Yuen, S. M. Lazarus, and S. S. Hanna, Nucl. Phys. A322, 168 (1979).
[39]J. Galin, D. Guerreau, M. Lefort, and Z. Tarrago, Phys. Rev. C 9, 1018 (1974); C. Ngo, thesis, Orsay Université Paris-Sud, 1975 (unpublished).
[40]D. Glas and U. Mosel, Nucl. Phys. A264, 268 (1976).
[41]R. Bass, Phys. Rev. Lett. 39, 265 (1977).
[42]M. Lefort, J. Phys. (Paris) Colloq. Suppl. II, 37, C5 (1976).
[43]U. Mosel, in *Proceedings of the International Conference on Nuclear Interactions, Canberra, Australia,* edited by B. A. Robson (Springer, 1978), p. 185.
[44]H.H. Gutbrod, M. Blann, and W. G. Winn, Nucl. Phys. A213, 267 (1973).
[45]D. Horn and A. J. Ferguson, Phys. Rev. Lett. 41, 1529 (1978).
[46]J. R. Birkelund, J. R. Huizenga, J. N. Dee, and D. Sperber, Phys. Rev. Lett. 40, 1123 (1978).
[47]L. C. Vaz and J. M. Alexander, Phys. Rev. C 18, 2162 (1978).
[48]R. A. Dayras, R. G. Stokstad, Z. E. Switkowski, and R. M. Wieland, Nucl. Phys. A261, 478 (1976).
[49]M. D. High and B. Cujec, Nucl. Phys. A278, 149 (1977).
[50]S. L. Tabor, D. F. Geesaman, W. Henning, D. G. Kovar, K. E. Rehm, and F. V. Prosser, Jr., Phys. Rev. C 17, 2136 (1978).
[51]S. E. Vigdor, in *Proceedings of the Symposium on Macroscopic Features of Heavy Ion Collisions,* Argonne National Laboratory, Report No. ANL/PHY-76-2 (Argonne National Laboratory, Argonne, Illinois, 1976), Vol. 1, p. 95.
[52]D. F. Geesaman, C. N. Davids, W. Henning, D. G.. Kovar, K. E. Rehm, J. P. Schiffer, S. L. Tabor, and F. W. Prosser, Jr., Phys. Rev. C 18, 284 (1978).
[53]D. G. Kovar, P. D. Bond, C. Flaum, M. J. LeVine, and C. E. Thorn, Bull. Am. Phys. Soc. 22, 66 (1977).
[54]H. Doubre, A. Gamp. J. C. Jacmart, N. Poffé, J. Roynette, and J. Wilczynski, Phys. Lett. 73B, 135 (1978).
[55]W. Scobel, H. H. Gutbrod, H. Blann, and A. Mignery, Phys. Rev. C 14, 1808 (1976).
[56]W. Scobel, A. Mignery, M. Blann, and H. H. Gutbrod, Phys. Rev. C 11, 1701 (1975).
[57]C. Ngo, B. Tamain, J. Galin, B. Beiner, and R. J. Lombard, Nucl. Phys. A24, 353 (1975).
[58]H. J. Krappe and J. R. Nix, in *Proceedings of the Third International Atomic Energy Symposium on the Physics and Chemistry of Fission, Rochester, 1973* (International Atomic Energy Agency, Vienna, 1974), p. 159.
[59]S. Cohen, F. Plasil, and W. J. Swiatecki, Ann. Phys. (N.Y.) 82, 557 (1974).
[60]A. Hertz, E. Essel, H. Körner, K. E. Rehm, and P. Sperr, Phys. Rev. C 18, 2780 (1978).
[61]C. Volant and J. P. Wieleczko, in *Proceedings of the XVII International Meeting on Nuclear Physics, Bormio, Italy, 1979* (unpublished).
[62]D. Glas and U. Mosel, Phys. Lett. 49B, 301 (1974).
[63]C. W. de Jager, H. de Vries, and C. de Vries, At. Data Nucl. Data Tables 14, 479 (1974).
[64]H. Flocard, S. E. Koonin, and M. S. Weiss, Phys. Rev. C 17, 1682 (1978).
[65]R. A. Broglia, C. H. Dasso, G. Pollarolo, and A. Winther, Phys. Rev. Lett. 40, 707 (1978).

[66]T. M. Cormier, J. Applegate, G. M. Berkowitz, P. Braun-Munzinger, P. M. Cormier, J. W. Harris, C. M. Jachcinski, L. L. Lee, Jr., J. Barrette, and H. E. Wegner, Phys. Rev. Lett. 38, 940 (1977).
[67]C. M. Jachcinski, T. M. Cormier, P. Braun-Munzinger, G. M. Berkowitz, P. M. Cormier, M. Gai, and J. W. Harris, Phys. Rev. C 17, 1263 (1978).
[68]P. P. Singh, D. A. Sink, P. Schwandt, R. E. Malmin, and R. H. Siemssen, Phys. Rev. Lett. 28, 1714 (1972).
[69]O. Tanimura, in *Proceedings of the International Conference on Nuclear Structure, Tokyo, 1977,* edited by T. Marumori (Physical Society of Japan, Tokyo, 1978), p. 34.